Radiation and Eddy Flux Experiment 1995
(Reflex III)

Jörg Hartmann, Axel Bochert, Dietmar Freese, Christoph Kottmeier, Dagmar Nagel and Andreas Reuter

Jörg Hartmann
Axel Bochert
Dietmar Freese
Christoph Kottmeier
Alfred-Wegener-Institut für Polar- und Meeresforschung
Columbusstraße
D-27570 Bremerhaven

Dagmar Nagel
Alfred-Wegener-Institut für Polar- und Meeresforschung
Forschungstelle Potsdam
Telegrafenberg A43
D-14473 Potsdam

Andreas Reuter
GKSS Forschungszentrum Geesthacht GmbH
D-21502 Geestacht

Contents

List of Figures

List of Tables

Abstract

REFLEX III completed a series of aircraft based experiments in the marginal ice zone north of Svalbard. A summer campaign REFLEX III took place from 15 June to 30 July 1995 and focussed on studying the low-level arctic stratus over sea ice. The experiment was carried out in cooperation with GKSS, Geesthacht, and AWI-Potsdam.

The aircraft instrumentation comprised four cloud particle probes, a sun-photometer, Eppley radiometers, colour line scanners and the turbulence probe Meteopod.

In the first 4 weeks Polar 4 flew single missions for cloud physics, sun-photometer, radiation studies and some line scanner recordings. In the last three weeks Polar 2 equipped with the turbulence probe was also available and 5 synchronised missions were flown.

1. Introduction

The experiment REFLEX III (Radiation and Eddy Flux Experiment) was conducted to study the effects of low level — mainly stratiform — clouds or Arctic Haze on the vertical radiative fluxes over various sea ice conditions in summer. Clouds and surface characteristics govern the radiation budget of the lower atmosphere and of the air-sea interface and thus critically affect the sea ice development in polar regions. The field work based on measurements with two suitably equipped research aircraft, Polar 2 and Polar 4 of Alfred Wegener Institute for Polar and Marine Research (AWI).

REFLEX III closes a series of three experiments in the marginal ice zone north of Svalbard all focussing on atmospheric boundary-layer processes. After an autumn experiment in September/October 1991 and a late winter experiment in March 1993, the summer campaign REFLEX III took place from June to August 1995. REFLEX I and REFLEX II concentrated on field and numerical model investigations of the atmospheric turbulence and the dynamics of convection in the lower atmosphere and on the effects of the lower boundary conditions on the ocean-atmosphere exchange processes.

During summer an almost permanent stratus cloud cover affects the meteorological conditions in the Central Arctic. It reduces the shortwave insolation and enhances the atmospheric counterradiation at the surface. When the daily sum of solar radiation is large, the shortwave cloud extinction may prevail over the longwave heating effect on the surface. The ice conditions are set by small net freezing in leads and polynyas and a generally smaller ice covered area. The large fraction of areas with a low albedo causes the larger sensitivity of sea ice regions to changes of the shortwave radiation budget.

Both aircraft carry upward- and downward looking pyranometers and pyrgeometers to detect the radiative effects of clouds. The instruments and the observational techniques have been extensively proven during REFLEX I and REFLEX II so that highly accurate radiation fluxes were obtained during coordinated flights above, below and within clouds. Furthermore, vertical radiation profiles were measured during ascents and decents of the aircraft. In addition to the radiative quantities the optical thickness (aerosol load) of the air column above flight level was measured with a sun photometer and cloud particles were observed by an FSSP (Forward Scattering Spectrometer Probe). Detailed information on the partly or totally ice covered sea surface were gained by downward looking line scan cameras in three visible spectral bands on both aircraft. The surface morphology (roughness) was detected by a laser altimeter. The vertical distribution of air temperature, relative humidity and the wind vector was measured during ascents and decents of the aircraft. Polar 2 also carried a gust probe, called Meteopod, under one of its wings which provides reliable values of the turbulent vertical fluxes of momentum, sensible and latent heat.

2. Scientific Objectives

2.1. Radiative effects of stratus clouds on the sea ice

The total shortwave extinction caused by a stratus cloud under prescribed in-solation at the cloud top depends on the cloud thickness, on the type and size distribution of liquid and solid cloud particles and on the surface albedo.

The measurements are performed in a way that the necessary input and verification data for radiation transfer models of the Arctic atmosphere are obtained.

2.2. Turbulent exchange of heat, momentum and water vapour

In addition to the radiative exchange between clouds and sea ice, energy is trans-ported by turbulent fluxes. The turbulent fluxes are enhanced when cold air is advected over regions of low ice concentration, i.e. in polynyas and regions in the marginal ice zone. The turbulent fluxes are determined directly with the Mete-pod system under the wing of Polar2 and indirectly from wind- and temperature soundings of the aircraft.

The flight patterns are arranged to obtain data sets, which are adequate for the forcing and validation of the mesoscale atmospheric model METRAS, which is particularly designed to simulate the atmosphere over the marginal sea ice zone.

2.3. Acquisition of ground truth data for the satellite remote sensing

The camera data obtained in the shortwave and in the terrestrial bands, laser altimeter data, and data on cloud properties will be used for comparisons with different satellite sensors frequently used in Arctic regions. They comprise chan-nels 3 - 5 of the NOAA series (detection of thin clouds and surface thermometry), the SAR-instruments of ERS-I and ERS-II (scattering and structural properties of sea ice) and the passive microwave SMM/I-sensor (sea ice concentration, ice age estimates).

2.4. Photometer

Aerosols are an important component of the atmosphere. The knowledge of the horizontal, vertical and temporal distribution of the Arctic aerosol and especially its influence on the radiation fluxes is very important for the understanding of climatological processes.

The objective of sunphotometer measurements during the REFLEX III experiment was the determination of vertical aerosol profiles in the lower troposphere in the region of Svalbard (15°E 78°N) in summertime. 12 profiles of aerosol optical depth were measured during flights in the areas shown in Figure 1. Additionally ground based measurements were done. The calculation of the optical properties of the tropospherical aerosol in dependence of its vertical distribution will give us an information about its influence on radiation fluxes.

2.5. Line Scanner

Operating airborne line scanners enable to record the surface structure of sea ice over large areas with high resolution imaging data. Maps of ice concentration showing different types of sea ice can be derived from these data. The camera measurements have been carried out in close relation to meteorological measurements and satellite remote sensing. The validation of algorithms to calculate ice concentrations from satellite data is of extreme importance.

The coarse spatial resolution of the satellite data do not allow a direct comparison with ground measurements. Especially the spatial variation of the ice formation would result in high uncertainties. Airborne line scanners have the potential to bridge the gap between satellite images and the real ice concentration.
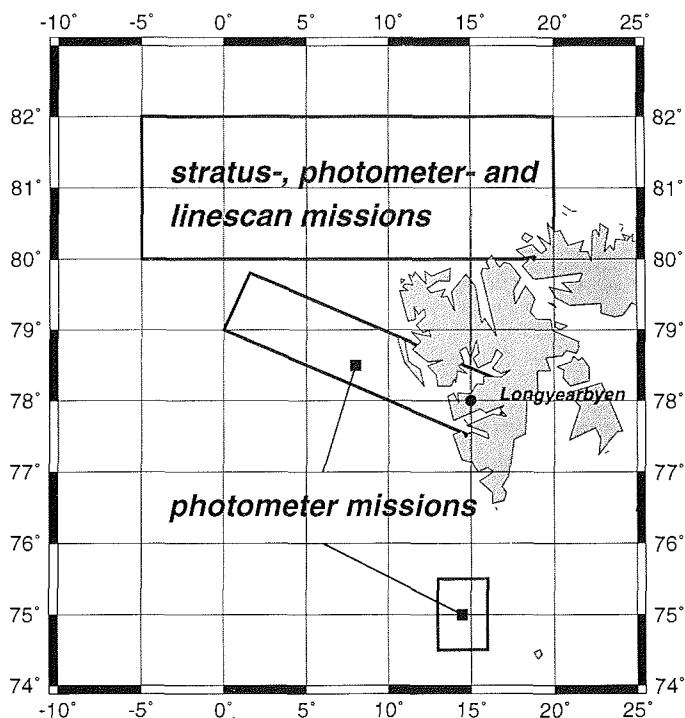
Figure 1: Region of the flight missions of REFLEX III.

3. Experimental Phase

REFLEX III took place from 16 June to 28 July 1995. In the first four weeks only Polar 4 was available and performed 17 flights. Polar 2 became available for the last two weeks where 5 synchronised missions with both aircraft were conducted. Initially flights were planned to start from Station Nord in Greenland and from Longyearbyen, Svalbard. However, due to logistical problems Longyearbyen remained the only base for flights. The main experimental region was the marginal ice zone to the north and north-west of Svalbard (between the 80th and 82nd parallel). Some missions for the sun photometer measurements were also flown in the west and south of Longyearbyen. Figure 1 shows the area where all missions were flown. A catalogue of all 22 flights is given in section 5.

Weather information was available from the meteorologist of *Det Norske Meteorologiske Institutt* (DNMI) at Longyearbyen and from maps received by fax. NOAA satellite pictures, processes at Tromsø Satellite Station, were transmitted by computer network.

3.1. Aircraft scientific equipment

The following table gives a list of the instruments on both aircraft. Parts of the equipment have been used in the previous experiments REFLEX I and REFLEX II and are described in the respective reports and in the User Handbook (Kottmeier, 1996). The new instruments and installations and some new calibrations are desribed in section 4.

Instrument	Polar 2	Polar 4
standard equipment (wind, temperature, humidity, GPS-position)	x	x
pyranometer and pyrgeometer (each up and down)	x	x
liquid water sensor	x	x
colour-linescan camera (new instrument)	x	x
laser altimeter	x	
Meteopod turbulence probing system	x	
sun photometer, optical window (new installation)		x
4 particle sondes (PMS, new installation)		x

3.2. Flight pattern

The following flight patterns were applied during REFLEX III:

A **sawtooth** pattern through stratus cloud decks to aquire vertical soundings (mainly Polar 4). This pattern was flown very frequently and provided a total of 430 vertical profiles.

Horizontal legs (both aircraft) below, inside and above cloud decks to measure radiation and particle distribution (Polar 4) and turbulent fluxes (Polar 2) at various heights. Horizontal legs were also flown in cloud-free situations to obtain sea ice pictures.

A **ladder** pattern (Figure 2) for sun photometer measurements with stacked legs at different heights but the same geographical position (Polar 4). Under clear sky conditions the flight pattern started at a level of 50 m, in cloudy conditions above the cloud top if it was below 500 m. Each leg was flown with a heading of 80° to the sun. A minimum of three measurements were made at each level. The procedure was repeated to a maximum height of 4000 m. The pattern ensured that pollution by the aircraft was always below the photometer and could not effect the measurements.

Synchronised circuits (Figure 3) around square boxes (both aircraft) at different heights below inside and above clouds. Polar 2 and Polar 4 synchroneously encircled the box of 15 km by 15 km size. The aircraft positions were offset by 180° which corresponds to a time offset of 10 Minutes. This pattern was flown on five days.
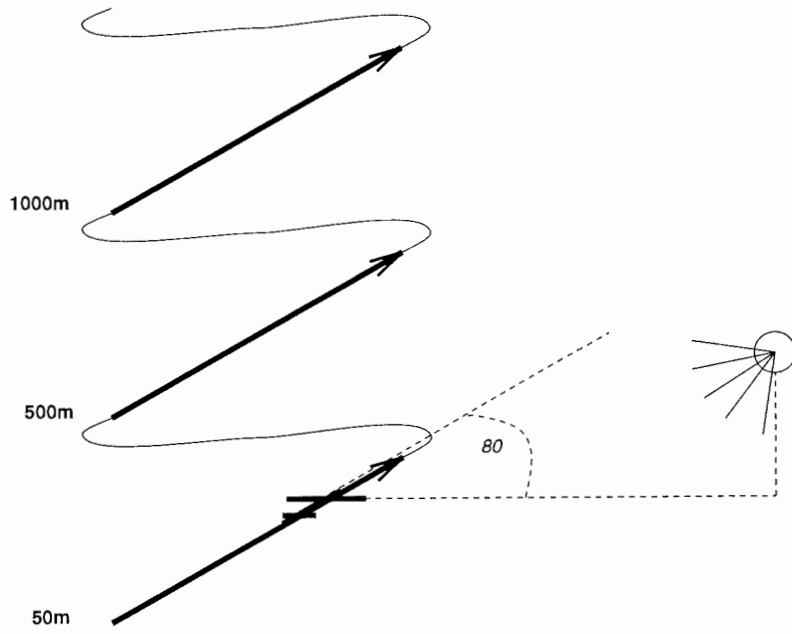
Figure 2: Ladder pattern.
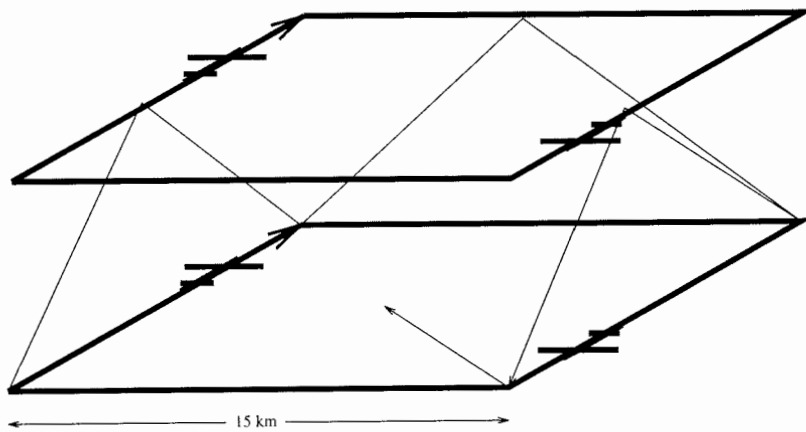
Figure 3: Box pattern.

4. New Instrumentation

A large part of the instrumentation was used for the first time on the Polar aircraft. This section describes the new instruments.

4.1. Photometer

Two types of sunphotometers were installed behind an optical window with well-known transmission properties. One, a fully automated device (on loan from the German Weather Service, Observatory Lindenberg), had 72 channels in the spectral range from 350 nm to 1200 nm (Leiterer and Weller, 1988). The lens had a viewing angle of 1°. A special amplifier system of the device allowed a dynamic range of 10^7 with a resolution of 10^4 in each stage.

The second is a commercial photometer developed by Schulz&Partner GmbH, Buckow. It is a half automated device with 14 channels in the range from 370 nm to 1100 nm. The lens is similar to that of the automated spectrometer and also has a viewing angle of 1°. The dynamic-range is 10^9.

Both instruments were mounted on an active solar tracker (also on loan from the German Weather Service, Observatory Lindenberg) to ensure an accurate orientation of the optical system towards the sun during the flight.

Calibration

The sun photometers were calibrated once a year by the Langley procedure on top of Zugspitze 2970 m MSL. The extraterrestrial values, used in the calculation of the optical thickness are determined by the Langley-plot. Furthermore every half a year, the device stability, especially of the used filters, was checked with help of a radiance- and irradiance etalon in the laboratory (Leiterer and Weller, 1993). The instruments allow to determine the aerosol optical thickness with an absolut error less than 0.001.

4.2. Color Line Scanner

High resolution line scanners were mounted on both aircraft to obtain accurate information on the sea ice characteristics. The systems were designed at Alfred Wegener Institute and consist of cross-track scanners to measure the intensity of surface signals perpendicularly to the flight track.

During REFLEX III the newly developed Color Line Scanner (Bochert and Holzschuher, 1995) was used in order to discriminate different types of sea ice and

Table 1: Particles sondes used during REFLEX III.

sonde	particle sizes (μm)	channels	resolution (μm)
PCASP-100X	0.1 – 3.0	15	0.02 - 0.5 unequally spaced
FSSP-100	2 – 32	15	2
FSSP-100	2 – 47	15	3
		number of photodiodes	
OAP-2D-GA2	10 – 640	64	10
OAP-2D2-C	25 – 800	32	25

to enable distinction between melt puddles, thin ice and open water. The Color Line Scanner (CLS) is sensitive in the visible spectral range and distinguishes simultaneously between red (0.40μm to 0.48μm), green (0.48μm to 0.58μm) and blue (0.58μm to 1.00μm).

The Color Line Scanner has the same field of view, 90°, as the Visible Line Scanner and the Infrared Line Scanner used in REFLEX II. It resolves each line in 1024 pixels. The altitude of the aircraft determines the width and the cross-track resolution of the images. The scanner has a maximum sampling rate of 50 lines per second. The along-track resolution is determined by the aircraft ground speed (typically 70 m/s, corresponding to 1.5 m). The data are stored on Digital Audio Tape (DAT), enabling four hours of acquisition time.

4.3. Particle Probes

For in-situ measurements of cloud properties and aerosols, Polar 4 was equipped with probes manufactured by PMS (Particle Measuring Systems INC., Boulder). Pylons designed by DLR, Oberpfaffenhofen were attached under each wing and each pylon carried two PMS probes. Considerable effort has been spent on an appropriate EMC-concept (Electromagnetic Compatibility) for the design of all cables (accomplished by Aerodata, Braunschweig) including development of a filter unit for the 28 VDC and 115 VAC power supplies. The PMS-probes were operated by personel of GKSS Forschungszentrum.

The probes used during REFLEX III ranged from a PCASP-100X to an OAP-2D2-C (Table 1). This concept allowed to measure the entire particle size range between 0.1 and 800 μm.

PCASP-100X

The PCASP-100X (Passive Cavity Aerosol Spectrometer Probe) measures particles in a size range between 0.1 and 3.0 μm. The 15 channels are spaced unequally in the following way:

channel	1	2	3	4	5	6	7	8	9	10	11	12	13	14	15
size	0.10	0.12	0.14	0.17	0.20	0.25	0.3	0.4	0.5	0.7	0.9	1.2	1.5	2.0	2.5 - 3.0

The PCASP-100X laser is a HeNe (632.8 nm) high order multimode tube. Laser alignment is achieved with a sensitive adjustment on the crystal oscillator assembly. The probe uses a combination reflecting-refracting imaging system in its collecting optics. This light gathering system collects more than one-half the total light with over 2π steradians collecting solid angle. The method of particle input is with an aerodynamically focused jet which constrains particle flow to a 150 μm diameter stream surrounded by a filtered sheath flow. The sample is positioned at the focus of a 5 mm focal length parabolic mirror and after reflecting off a 45° flat mirror, it is refocused by an aspheric lens. A single photodiode detector converts the collected light into signal photocurrent. To accommodate the large dynamic range of the probe, three independent gains are utilised.

Calibration of the PCASP-100X is accomplished by latex particles of different size, nebulised with an aerosol generator. The performance of all three gains is checked on a regular basis.

FSSP-100

The FSSP-100 (Forward Scattering Spectrometer Probe) from PMS provides 4 different size ranges to measure cloud droplets:

Range	0	1	2	3
size interval μm	2–47	2–32	1–16	0.8–8

To achieve a significant overlap with the optical array probes, only the ranges 0 and 1 had been used during REFLEX III. In each range the particles are classified into 15 equally spaced channels.

The beam of a 5 mW HeNe multimode laser is focused at the centre of the sampling aperture. In the absence of particles a central dump spot just before the collecting optics totally shuts the laser beam. Particles crossing the beam within the depth of field scatter light into the optics. The intensity of the scattered light, which is a function of the particle size and shape as well as the laser mode and the way through the beam, is measured with a photodiode. In front of this detector diode there is a beam splitter with a central dump spot and a second photodiode

behind. This annulus diode is used to control whether a particle was within the depth of field or not. Light scattered by particles within or near by the focal plane is masked by the dump spot whereas out of focus particles scatter light onto the annulus diode. To define the depth of field electronically, the annulus voltage must be lower than the signal voltage to accept a particle puls.

For spherical particles, Mie theory gives a relation between the scattered energy and particle size. Based on such calculations, the measured intensities are interpreted as particles sizes by the probe electronics.

The sampling volume of the FSSP-100 is given by the product of the flight distance per sampling interval and the effective sampling area. This sampling area is determined by the laserbeam width (0.23 mm) and the depth of field (2.20 mm), being 0.506 mm^2.

Due to this principle of operation, the FSSP-100 can give reliable results only in the case of pure water droplets. Ice particles with various shapes result in significantly different scattering functions. In the presence of ice crystals, this can result in an overestimation of the number density up to 500% (Gardiner and Hallet, 1985).

Commonly, calibration of the probe is accomplished by the use of glass beads of known diameter, thrown through the sample area of the probe. For this purpose we developed a device operating on the basis of an air jet pump, mounted on top of probe tube. Due to the known refraction index of the glass beads it is possible to convert the measured scattering intensities of the beads to water droplet sizes.

OAP-2D-GA2 (2D-Greyprobe)

The 2D-Greyprobe from PMS is the latest development of the Optical Array Probes. Shadow images of cloud particles in a size range of 10 to 620 μm are focused on a diode array with 64 elements which is read with a maximum repetition frequency of 5 MHz. The light source is a HeNe-Laser. The electronics provide a distinction between 4 different greylevels of the image:

intensity	0-24%	25-49%	50-74%	75-100%
greylevel	max	mid	min	none

The optical system of the probe contains a zoom-optic with magnifications between 15 and 20 and enables a maximum resolution of the array of 10 μm. The resolution in flight direction is given by the ratio of the particle velocity (true air speed) and the repetition frequency of the probe (slice rate).

Only particles passing the probe within the focal plane result in an image with a maximum degree of sharpness. Images of particles which pass the probe outside the focal plane are more or less blurred. The distance along the laserbeam, where crossing particles produce a recordable image, is called depth-of-field and

is a function of the particle size. The maximum depth-of-field is given by the distance of the probe tips (62 mm). The sampling volume of the probe is the product of the flight distance during the sampling interval, the depth-of-field and the effective array width and is itself a function of the particle size. The effective array width takes into account that the size of an image can only be determined in a unique way if the entire image is focused on the diode array. This means that the probability for large images to shadow an end element of the array is bigger than for smaller particles. Since images that obscure an end element are rejected during data analysis, the effective array width corrects the sampling volume for bigger particles.

Recent measurements (Reuter, 1994) show that the depth-of-field is 3.02 times larger than usually used. This has an important impact on the data analysis because the sampling volume of the greyprobe changes significantly.

Another problem is caused by out of focus particles which produce blurred images because the size of these images increases with increasing distance from the focal plane. The maximum image diameter can be up to 1.8 times bigger than the image diameter within the focal plane, causing an overestimation of the particle volume of up to 800%. Reuter (1994) developed a size correction technique for these particle images. So it is possible to compute the nominal particle diameter for out of focus particles with an accuracy of 94%.

Calibration of the probe is accomplished by a rotating glass disk with opaque spots on it simulating particles. This device can be attached to the probe tips and two micropositioner enable the adjustment of the disk in the depth of field. Spotsizes are available from 50 to 500 μm and therefore cover almost the entire size range of the probe.

OAP-2D2-C

The function principle of this probe is similar to this of the 2D-Greyprobe. There are only two major differences: The photodiode array of the 2D2-C consists of 32 elements instead of 64 and the 2D2-C uses a 50% threshold of the laser intensity resulting in two shadowlevels. Therefore, a correction technique for out of focus images can not be applied to the 2D2-C. This implies that the data of this probe can only be processed reliably for particles larger than approximately 300 μm which is the case in multi-layered boundary layer cloud decks.

5. Flight Catalogue

This section presents a catalogue of all flights during REFLEX III. Table 2 gives a brief listing of these flights, the following pages show the tracks of each flight, a satellite picture and a description of the situation. In the presence of clouds, a table gives the cloud top and bottom height in the measure area.

Table 2: Catalogue of flights during REFLEX III. The table lists: *date* of flight; *code* assigned for each day for use in the nomenclature of flight legs; *Polar 2*, *Polar 4* participation of the respective aircraft; *stratus* type of stratus pattern, implies cloud particle and radiation measurements; *photometer* pattern; *linescan* flight over SAR-scene; *calibration* pattern flown.

date	code	Polar 2	Polar 4	stratus	photometer	linescan	calibration	remarks
16 June	a	x						test
17 June	b	x		L				
19 June	c	x			x			
20 June	d	x		L	x	x	x	
22 June	e	x		L				
24 June	f	x			x	x		
25 June	g	x			x			
27 June	h	x		L	x		x	(radiation)
3 July	i	x		||				
4 July	j	x		L	x			
8 July	k	x		L		x		
9 July	l	x		L	x			
10 July	m	x			x			6700 m
11 July	n	x		|				
12 July	o	x		L				
14 July	p	x						test
15 July	q	x		L	x	x		
18 July	r	x	x	box				
20 July	s	x	x	box	x			
23 July	t	x	x	box	x	x	x	
24 July	u	x	x	box				
28 July	v	x	x	box		x		

17 June 1995

A weak high-pressure system with small gradients prevailed over Svalbard and the marginal ice zone.

An L-shape stratus pattern was flown over the ice and photometer measurements were performed off the entrance of Isfjord between the surface and 3600 m height.

cloud tops	880 – 1100 m
cloud bottom	150 – 560 m
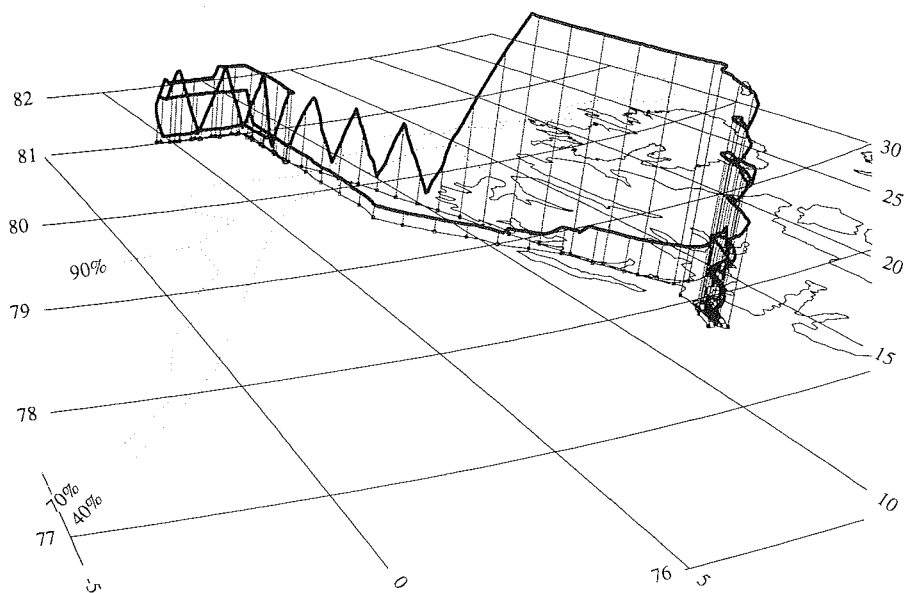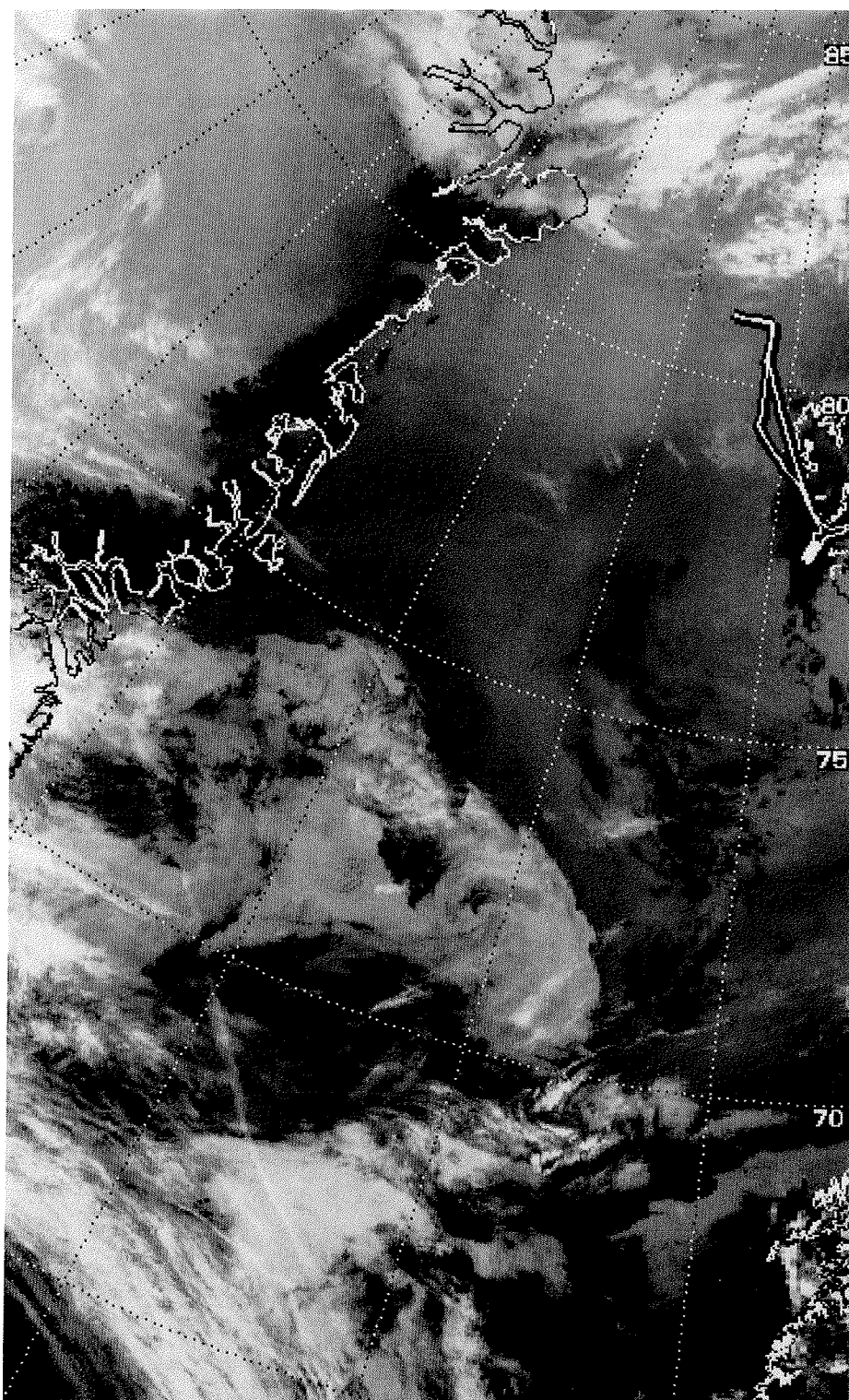
19 June 1995

The fligth mission concentrated on photometer measurements in the south, at 74°40'. A ladder pattern was flown at levels between 60 m and 3700 m.
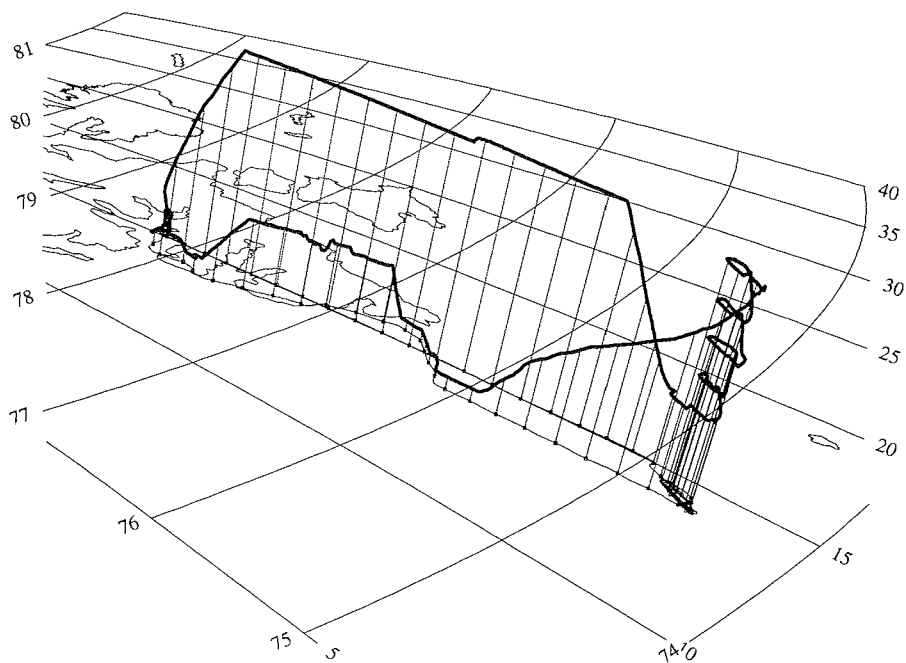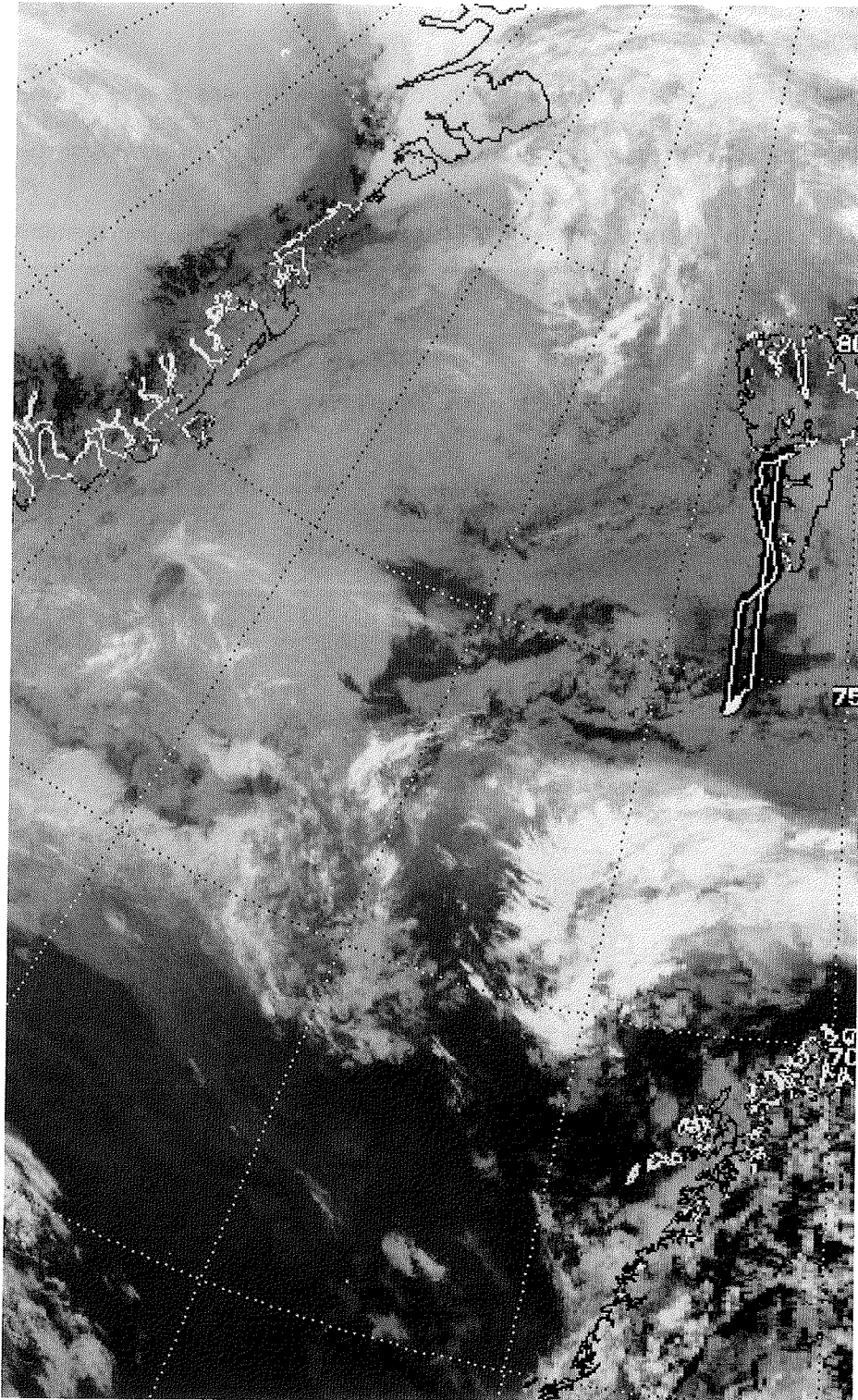
20 June 1995

The high pressure situation over Svalbard continued. The sea ice north of Sval-
bard was covered by low stratus, thin near the ice edge and intensifying towards
the north. Over the ice the stratus was very homogeneous and extended between
800 m and 1100 m.

An L-shape pattern was flown in 7 heights in the region of the homogeneous
stratus. Photometer measurements were made at several locations and some
calibration flights for the pyranometers.

cloud tops	720 – 1150 m
cloud bottom	610 – 860 m
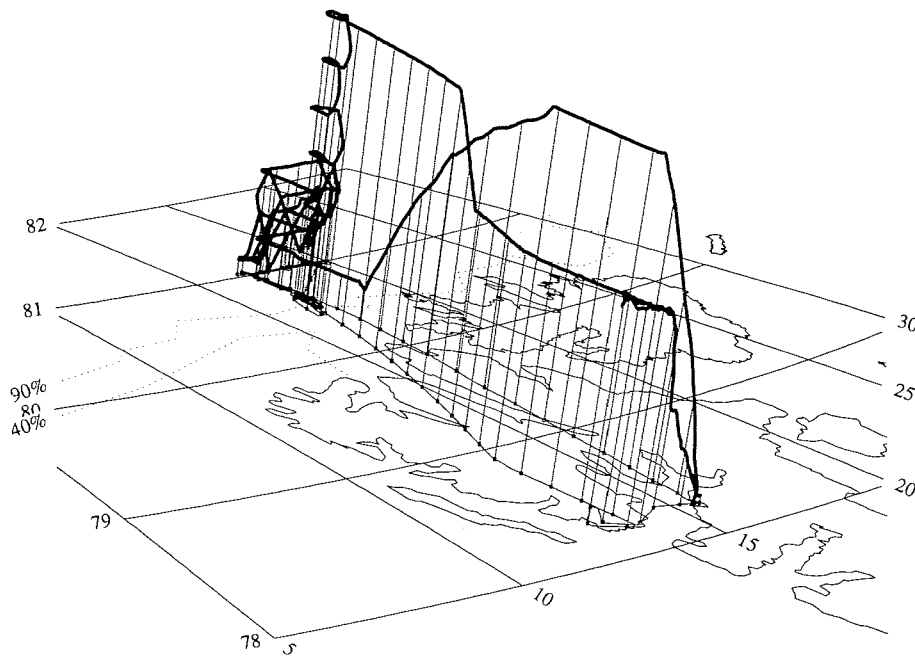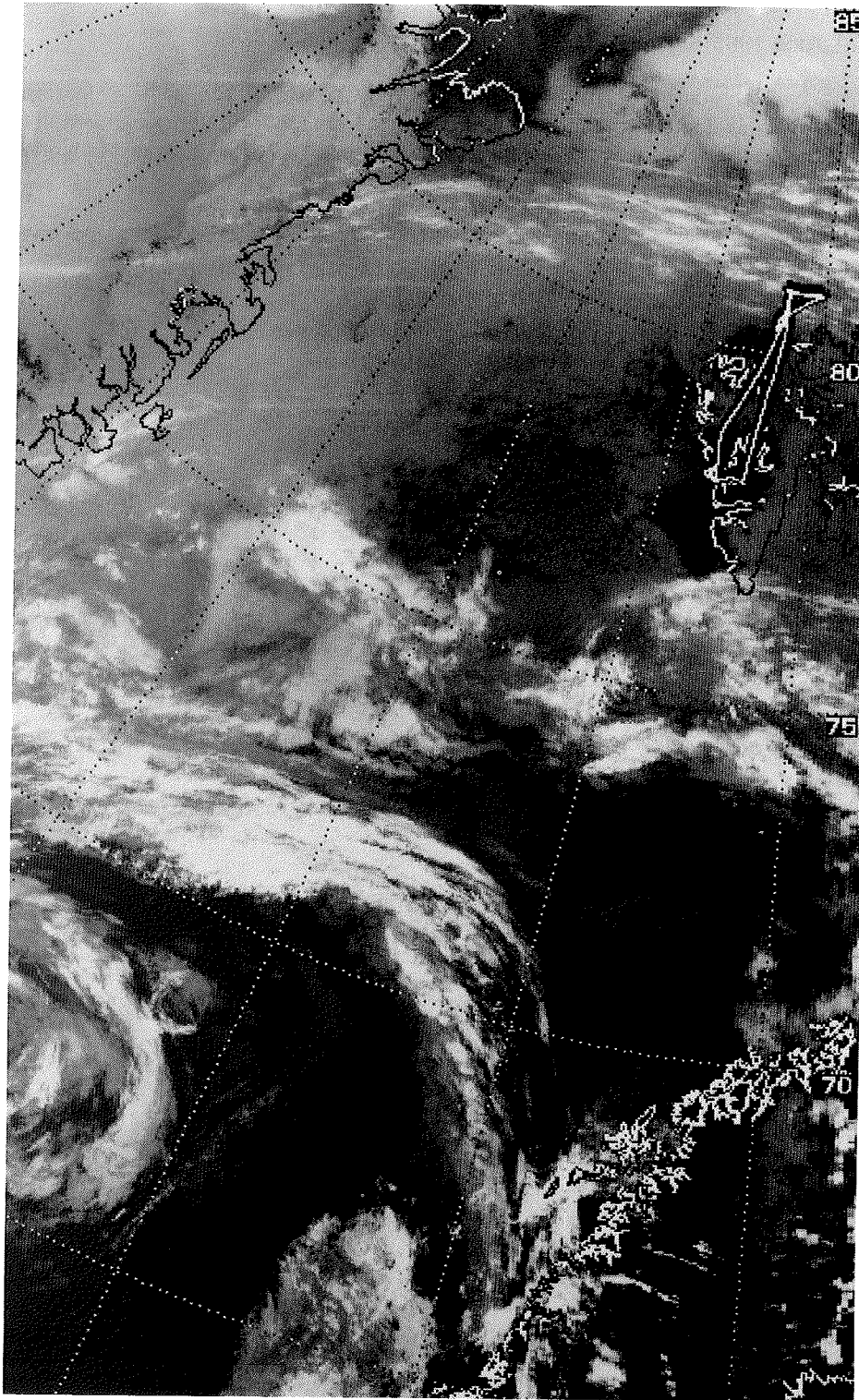
22 June 1995

The high pressure cell of the recent days moved towards the east. A low approached Svalbard from the south with a warm front crossing Longyearbyen during the day. The ice north of Svalbard was still covered by low stratus, but higher clouds were also present.

12 legs were flown between 80°30' N and 81°N as saw-tooth patter and level flights in different heights.

	layer 1	layer 2
cloud tops	720 – 1050 m	1560 – 1700 m
cloud bottom	390 – 700 m	1420 – 1500 m
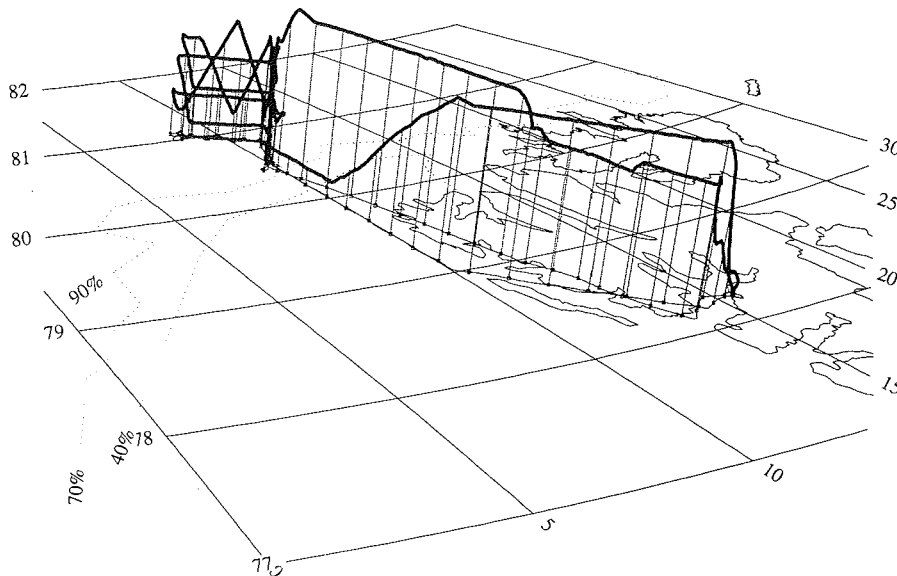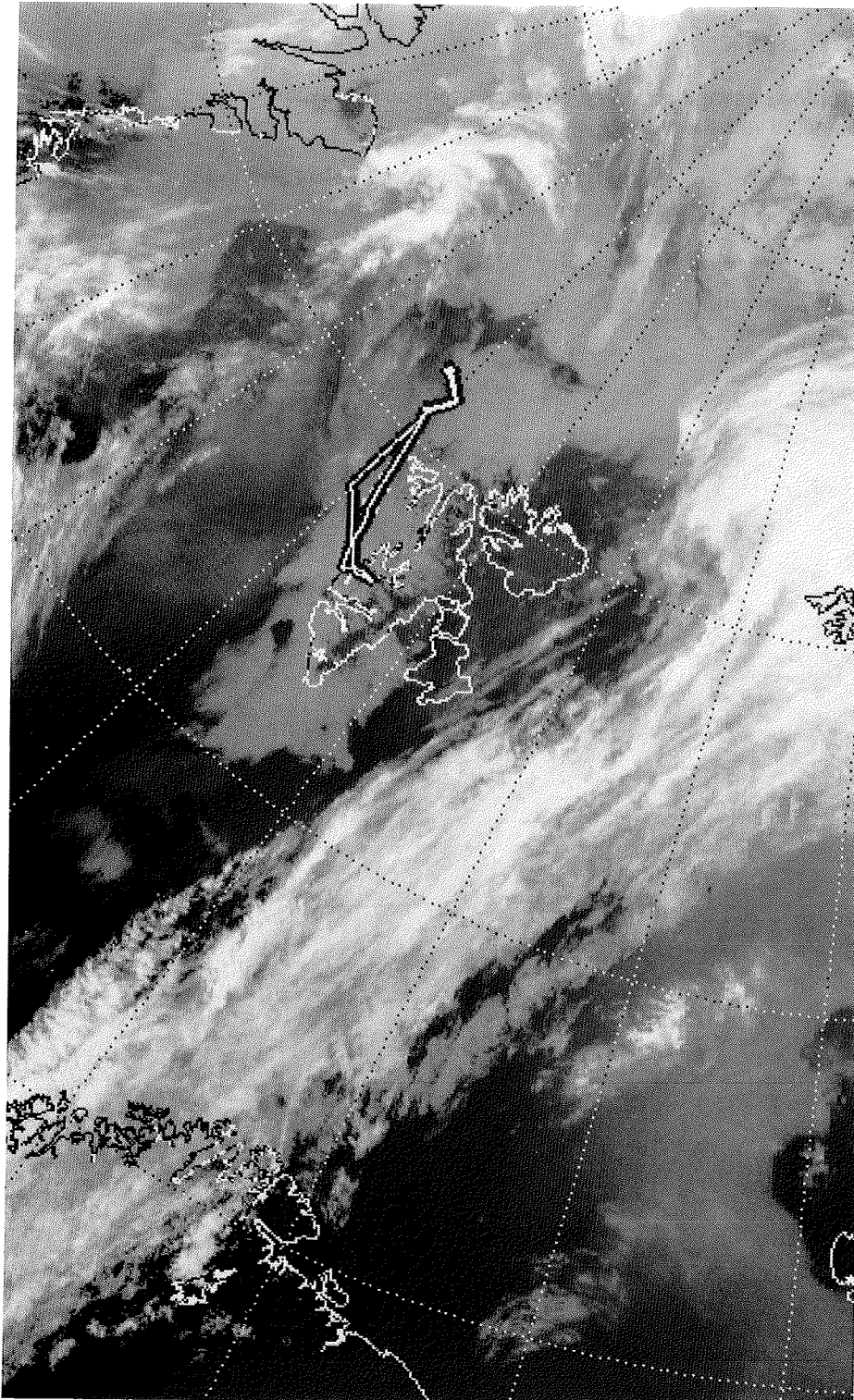
24 June 1995

After the passage of a low pressure system on the 23 June complex cloud system prevailed in the region.

Some legs of an L-pattern were flown over the ice but aborted due the the complexity of the clouds. Photometer measurements were carried out in 5 heights.

cloud tops	2200 – 2300 m
cloud bottom	
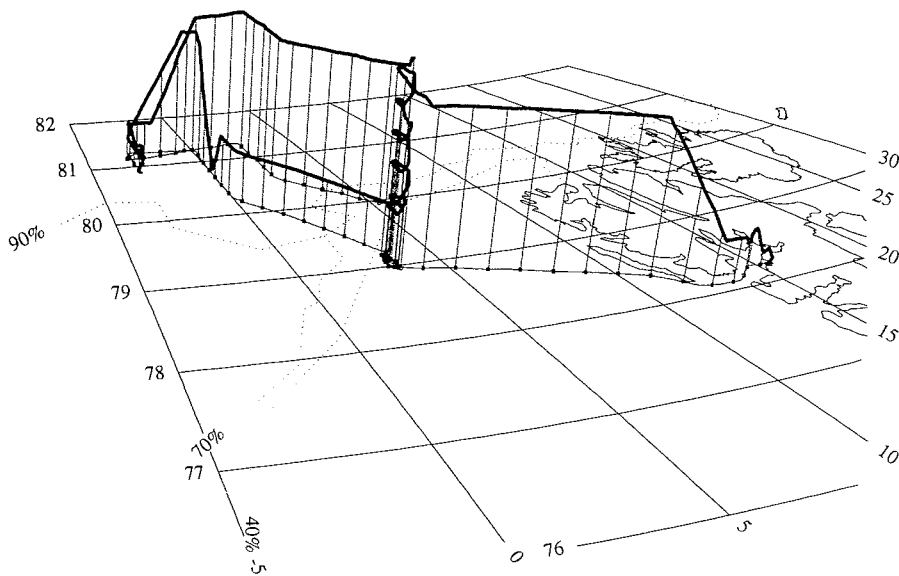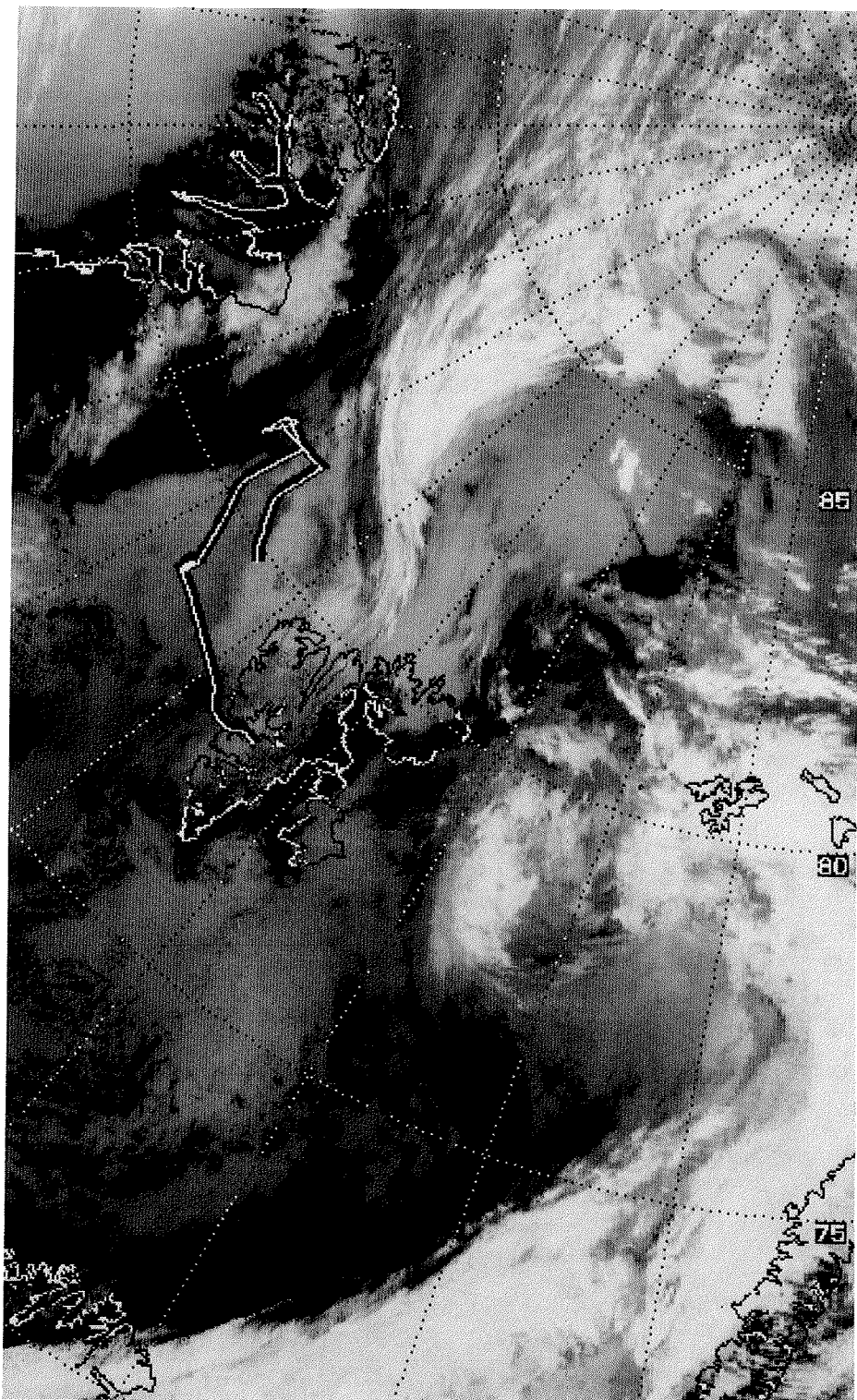
25 June 1995

The day was used for extensive measurements with the photometer. A ladder-pattern was flown with 11 height levels.
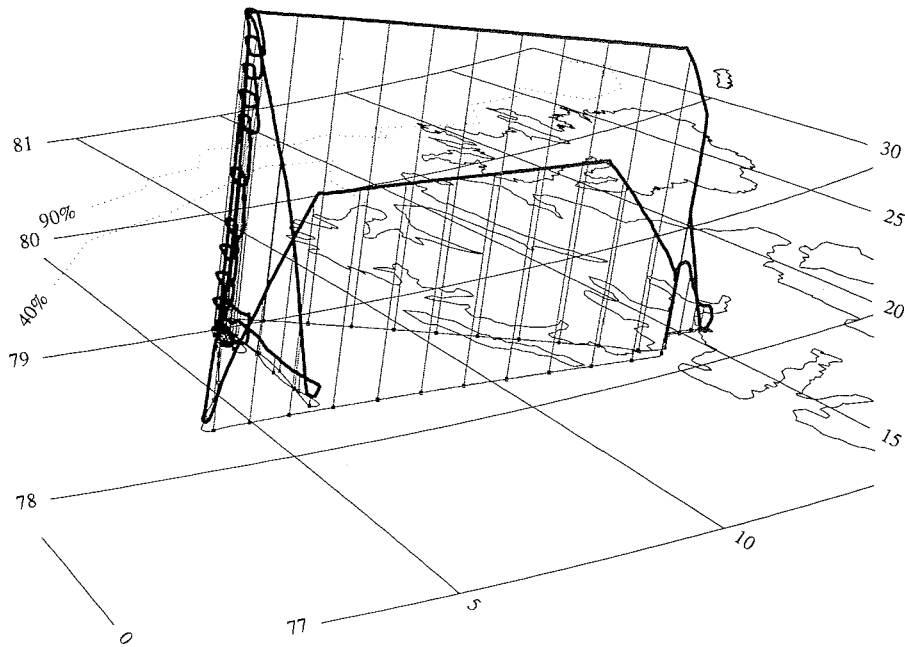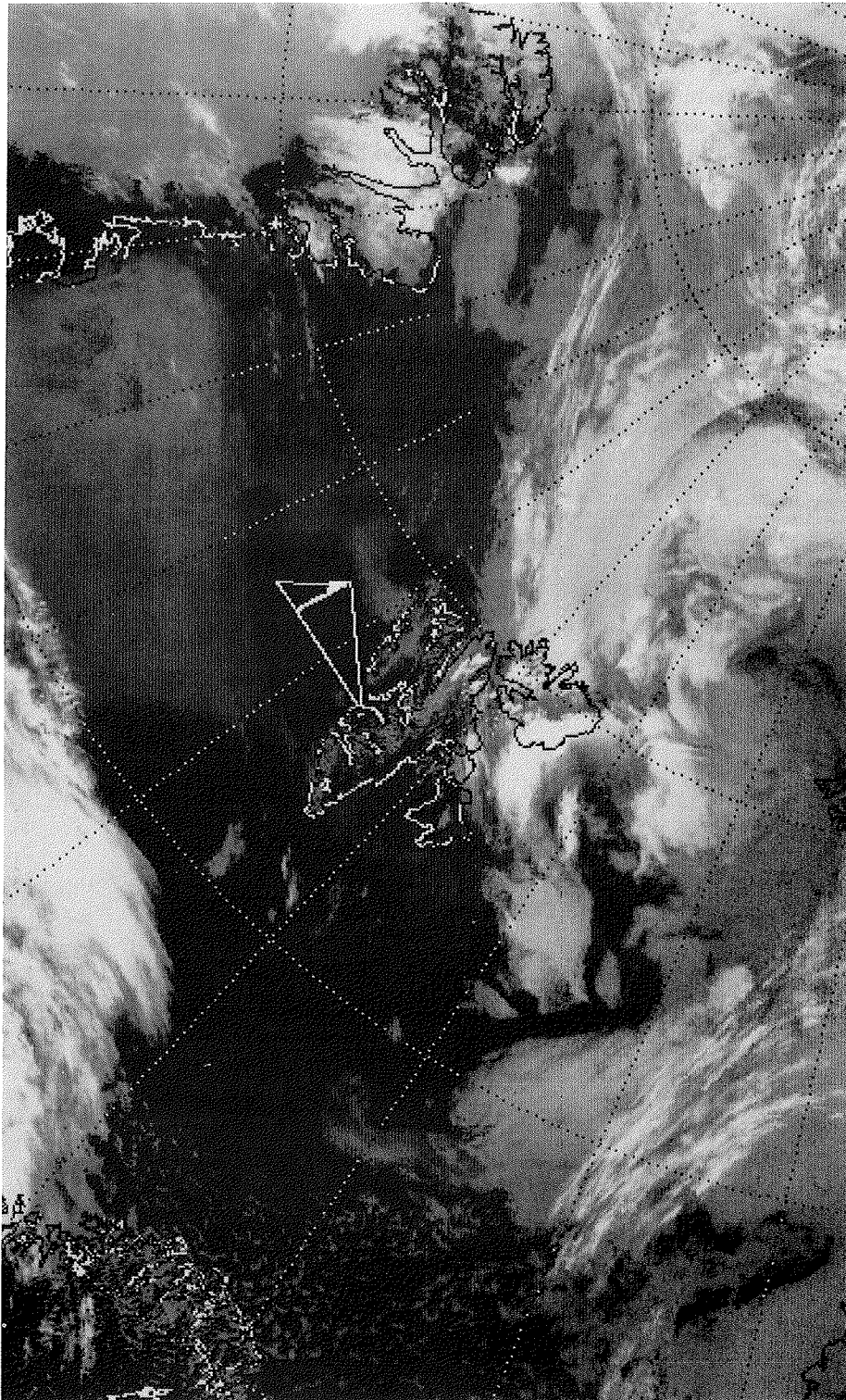
27 June 1995

The region is situated between a small low pressure system north of Svalbard and
high pressure over Greenland. Low stratus over the ice of the East-Greenland-
Current touched the ground. The area in the immediate west of Svalbard was
cloud-free.

An L-pattern stratus mission was flown over the ice before the east coast of
Greenland in heights between 60 and 170 m. Near Svalbard a ladder pattern was
flown for photometer measurements.

cloud tops	120 – 150 m
cloud bottom	< 60 m
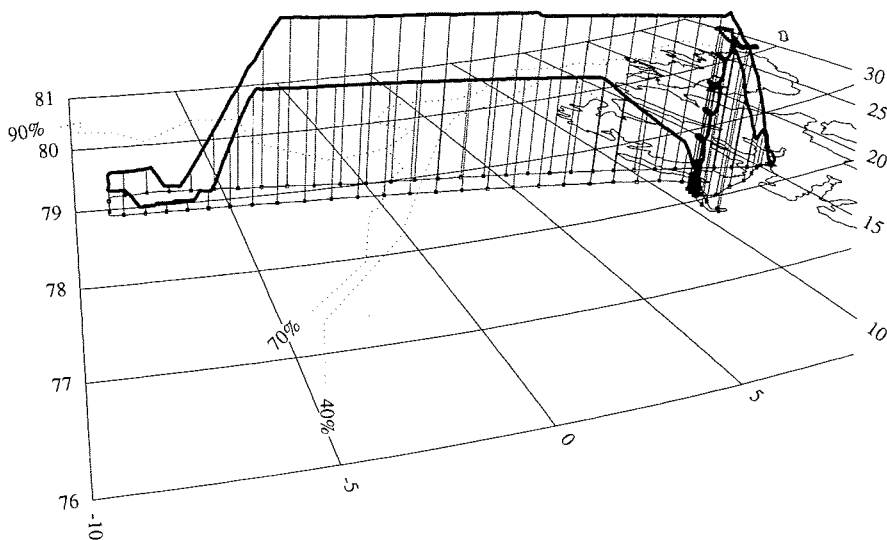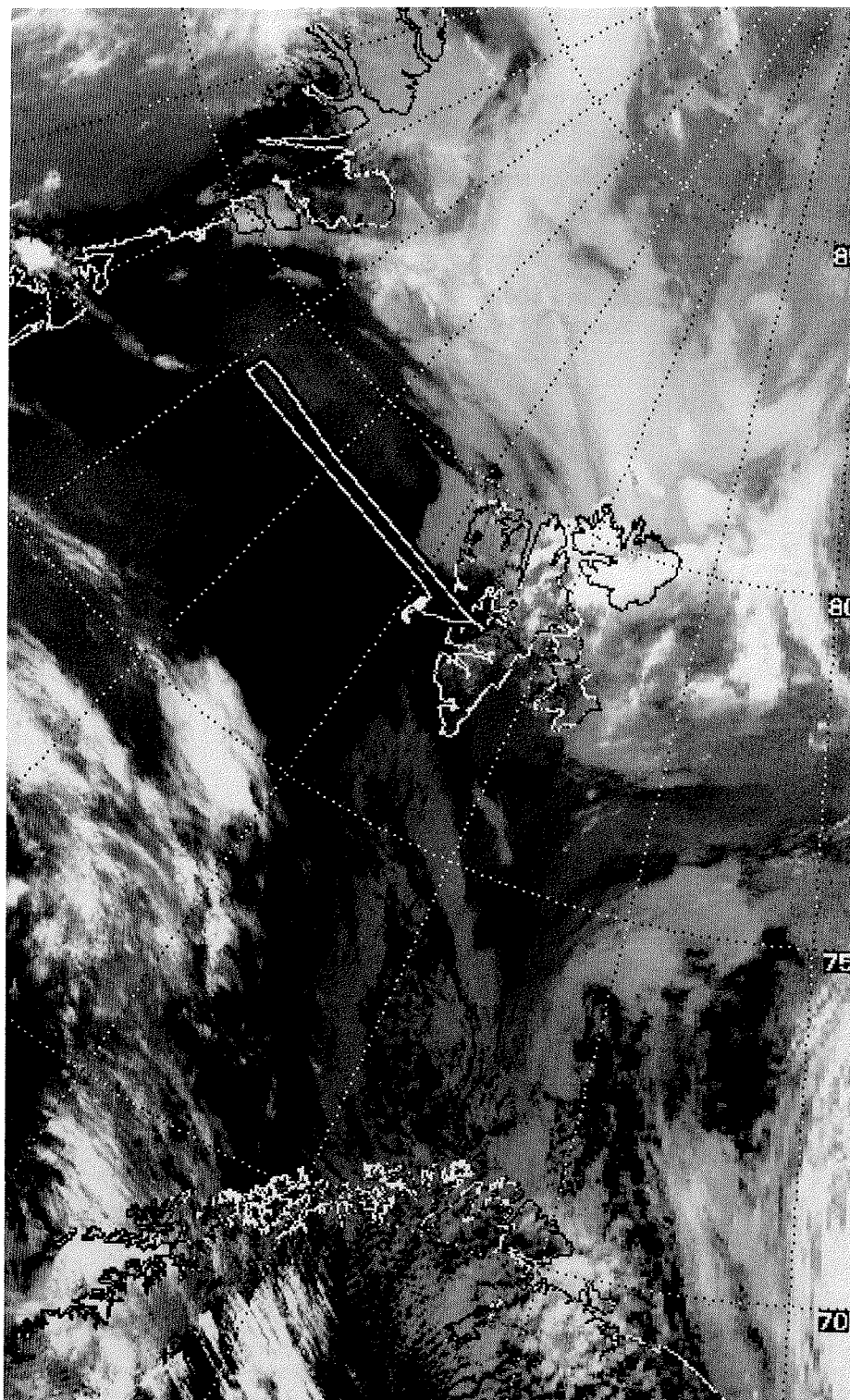
3 July 1995

Influenced by a weakening low pressure system over the ice the situation is characterised by complex could structures.

A stratus mission with parallel legs in several heights is flown in the north of Svalbard.

	layer 1	layer 2
cloud tops	330 – 600 m	1000 - 1460 m
cloud bottom	200 m	720 - 850 m
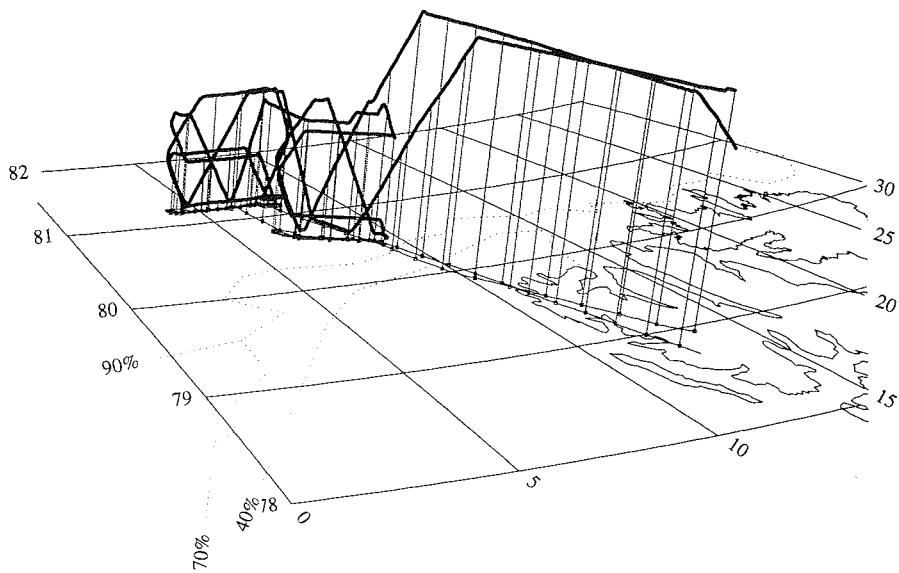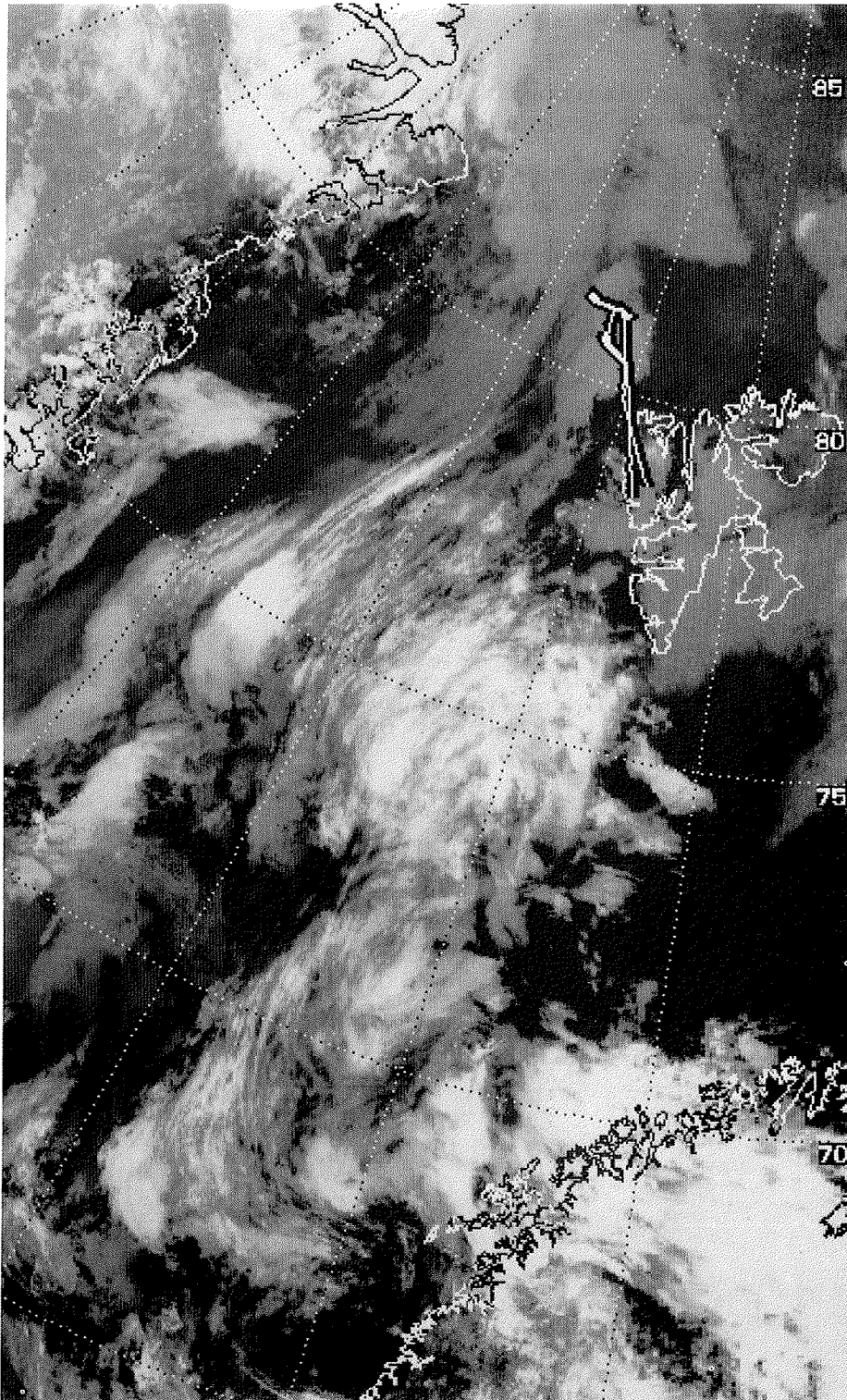
4 July 1995

The situation is controlled by high pressure over the Central Arctic and a low pressure system over Norway.

An L-pattern is flown over the ice in 4 levels and a ladder pattern for photometer measurements between 600 m and 3700 m.

cloud tops	420 – 530 m
cloud bottom	70 m
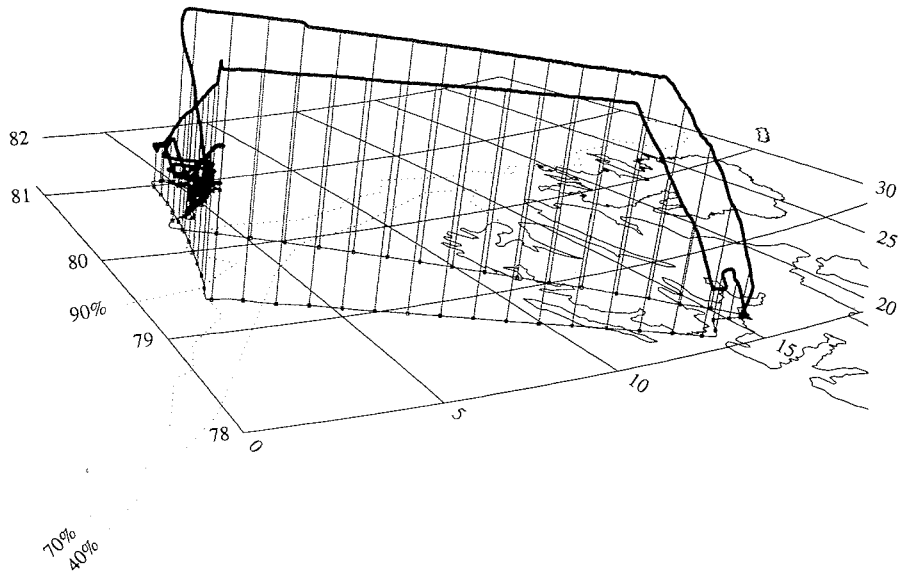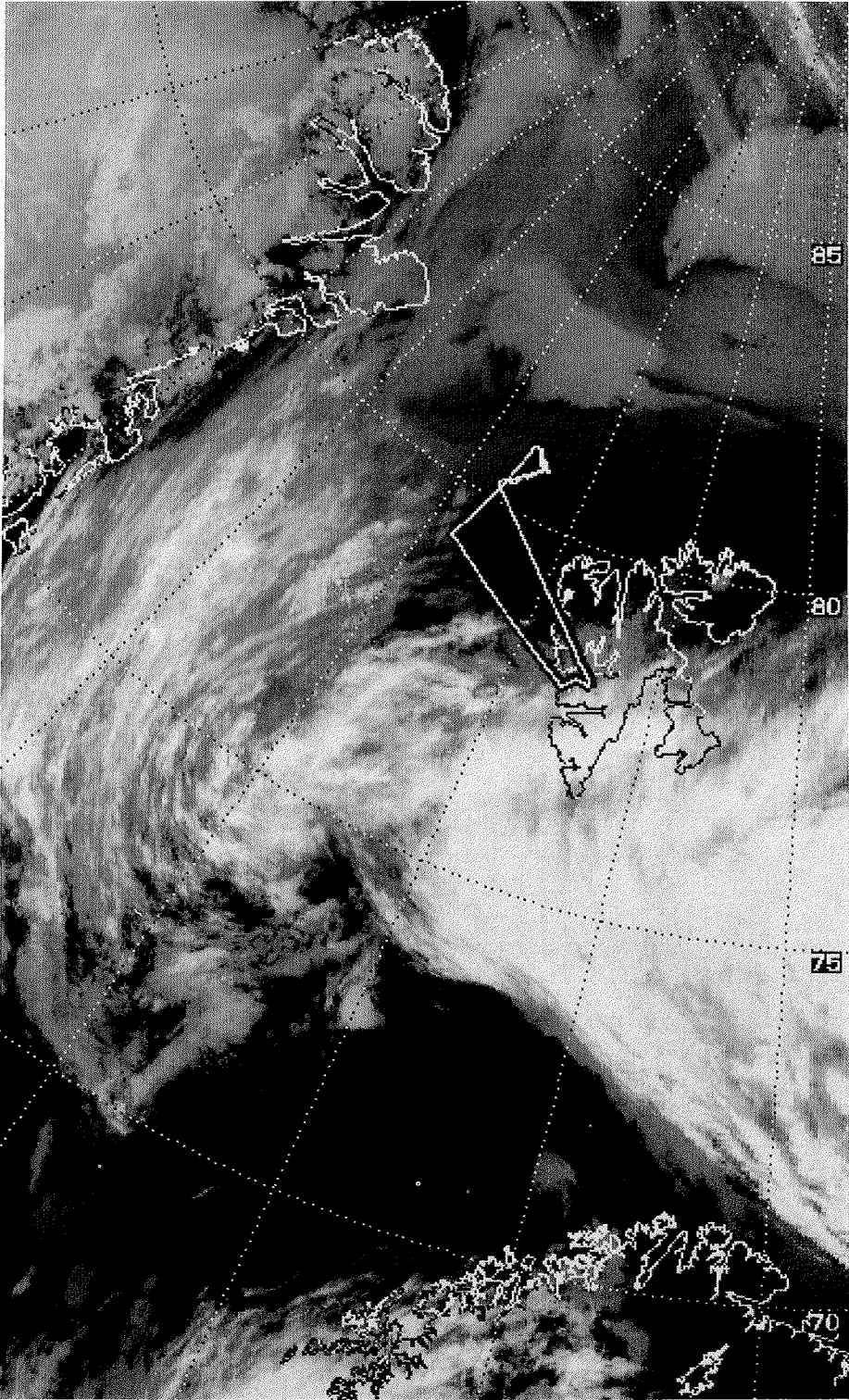
8 July 1995

With a south-easterly airstream cirrus clouds formed over Svalbard and moved northward ahead of an approaching low-pressure system over Norway. A second low-pressure system was situated at the east coast of Greenland.

The measurements over the ice began with three legs over a SAR-scene to gather data with the linescanner followed by an L-shaped stratus pattern.

cloud tops	150 – 260 m
cloud bottom	< 60 m
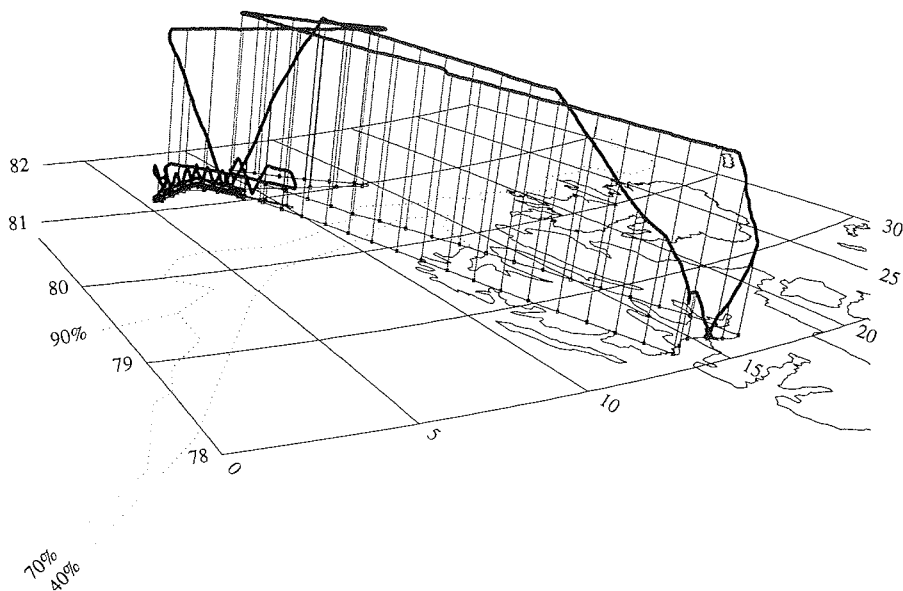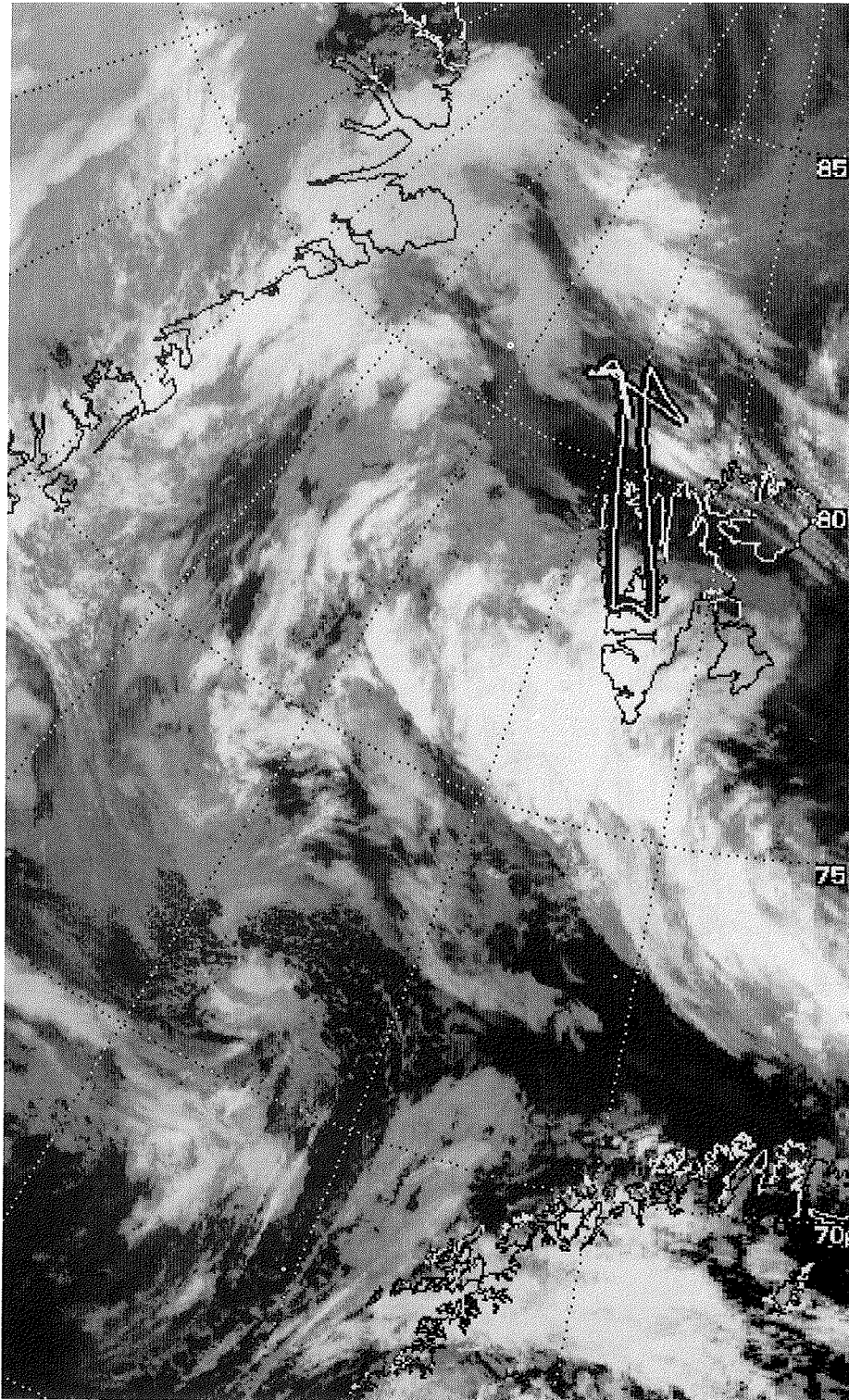
9 July 1995

High pressure over Greenland and a low-pressure system south-east of Svalbard lead to north-easterly winds in the region. The ice is largly coverd by low-level stratus and fog. No high or mid-level clouds are present.

An L-shaped stratus pattern between 60 m and 850 m and a photometer mission between 670 m and 3700 m were flown.

cloud tops	600 – 700 m
cloud bottom	< 60 m
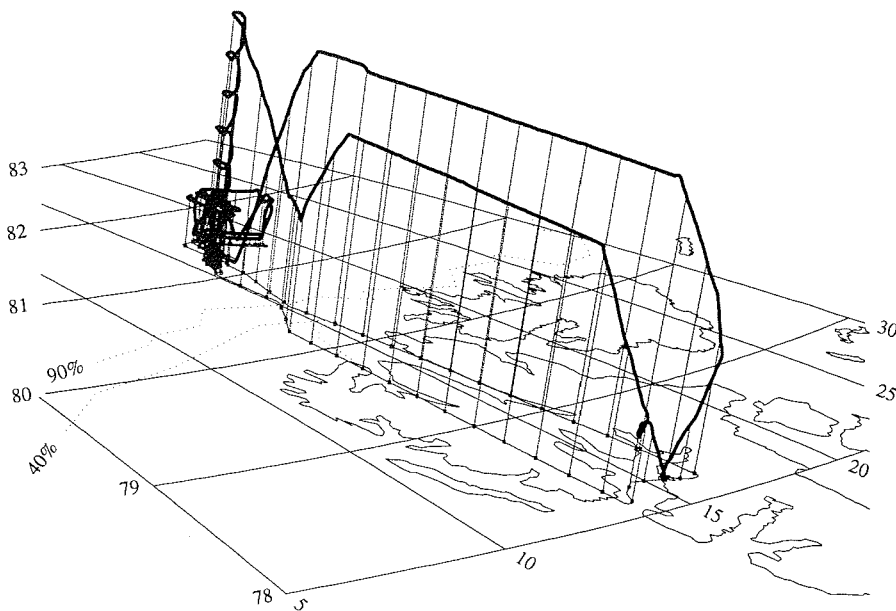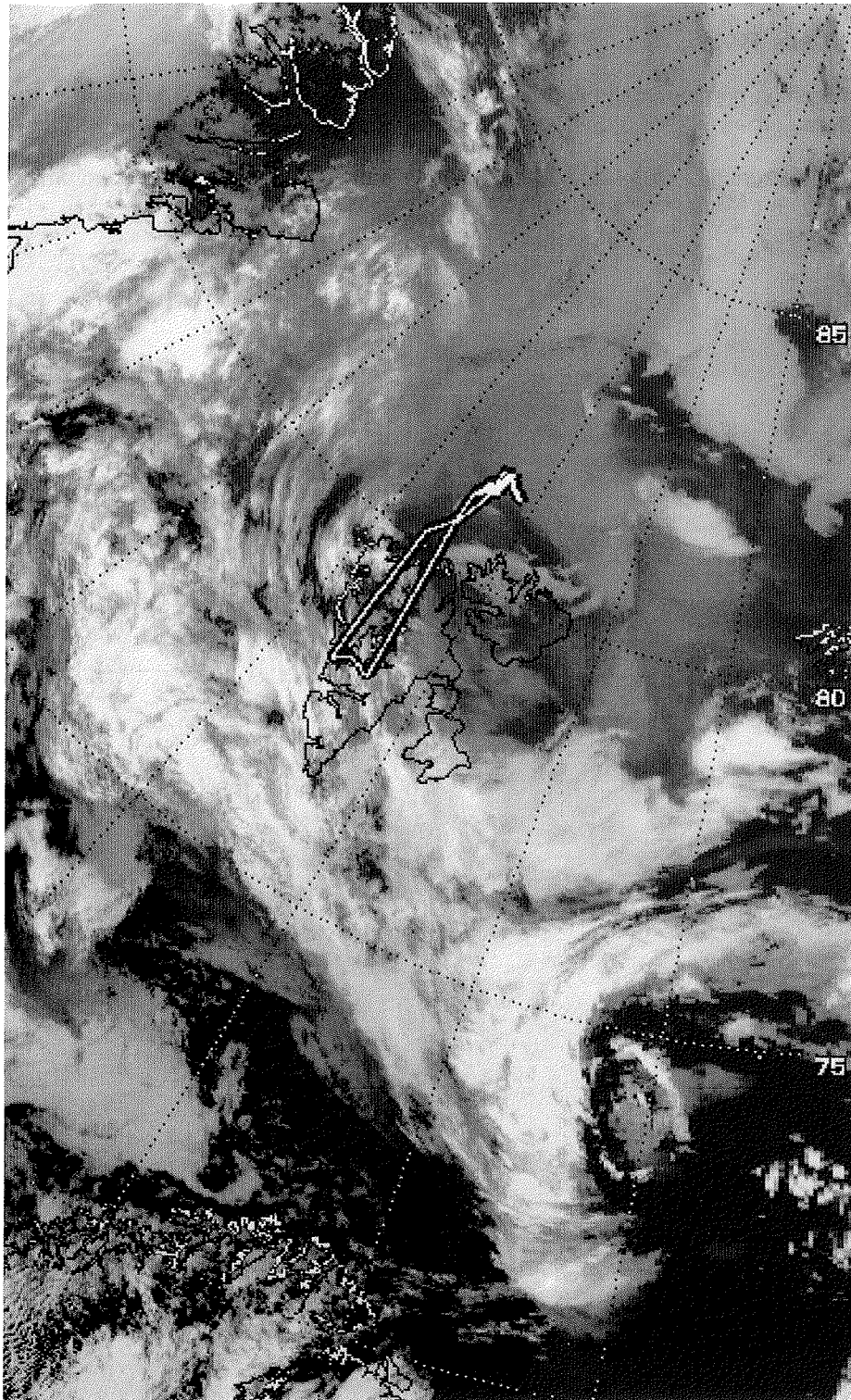
10 July 1995

The high-pressure cell over Greenland gains influence in the west while a cold front of the low east of Svalbard is situated over the ice in the north.

The absence of high and mid-level clouds is used to perform a high photometer mission to a maximum level of 6700 m.
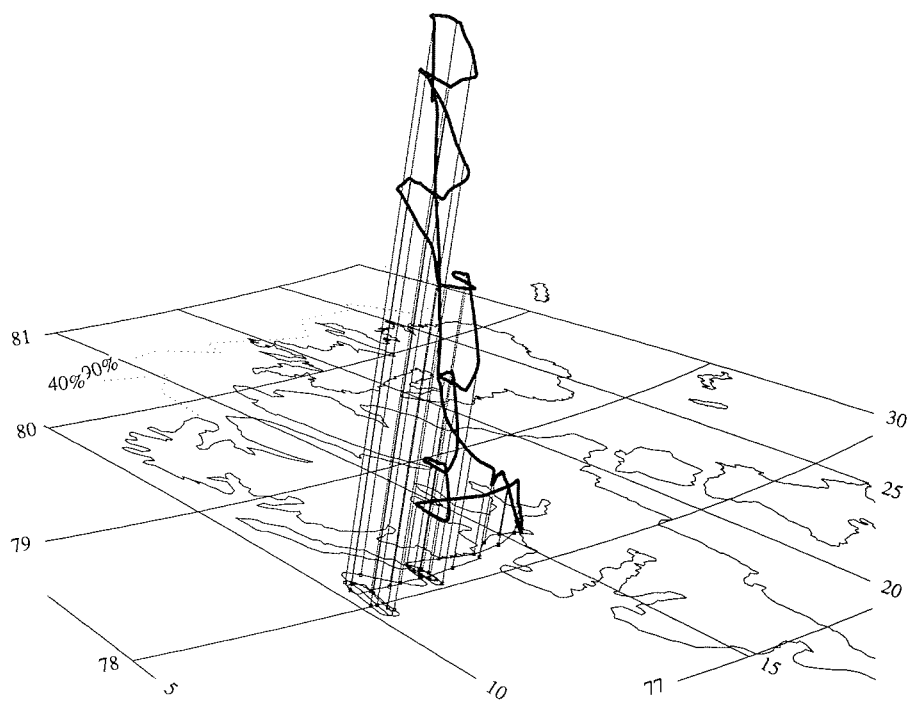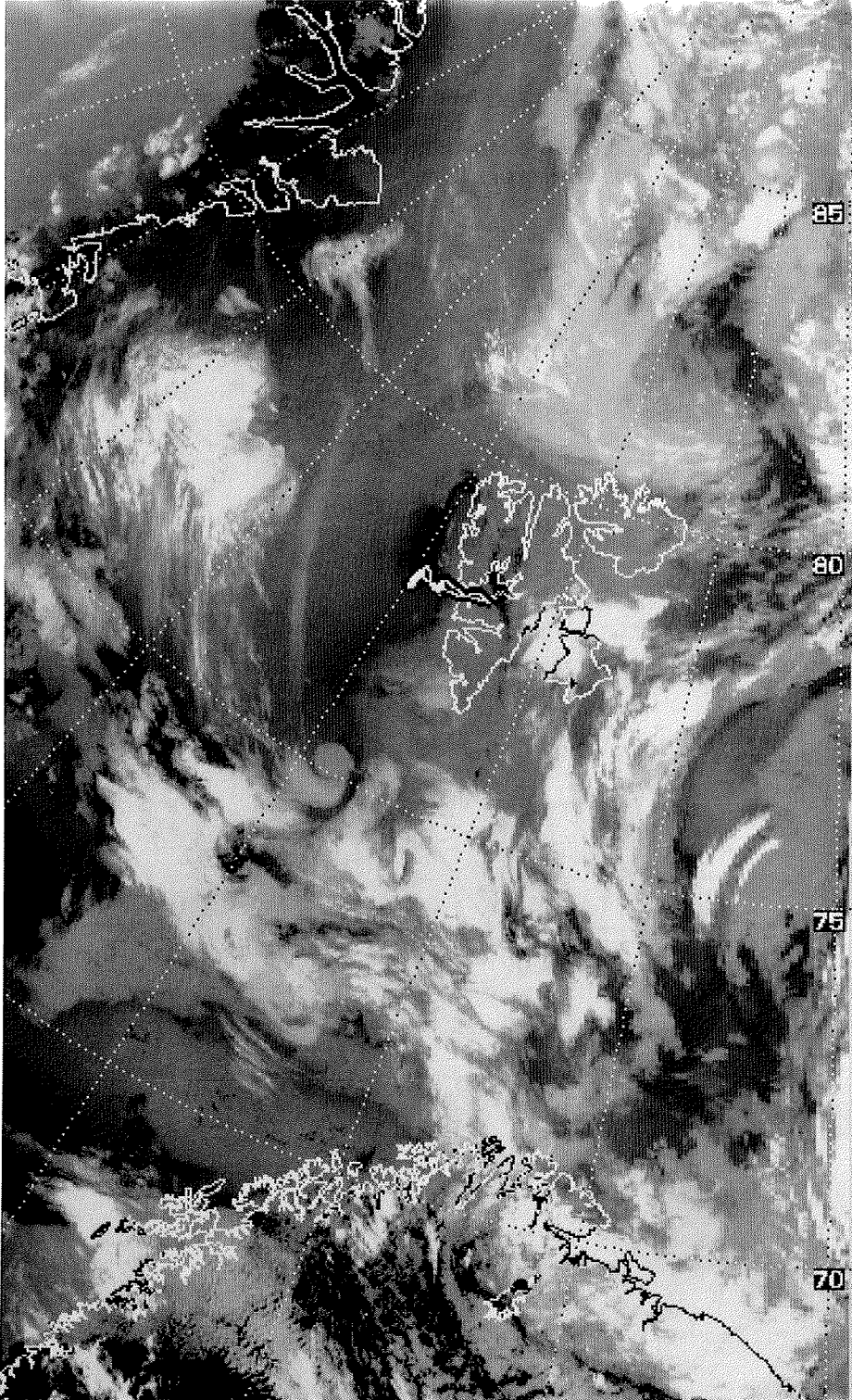
11 July 1995

A low pressure system was approaching Svalbard from the south east.

A complex and inhomogeneous stratus system was encountered over the ice. The stratus was surveyed by saw-tooth patterns and horizontal legs in 11 levels.

cloud tops	1260 – 1600 m
cloud bottom	< 60 m
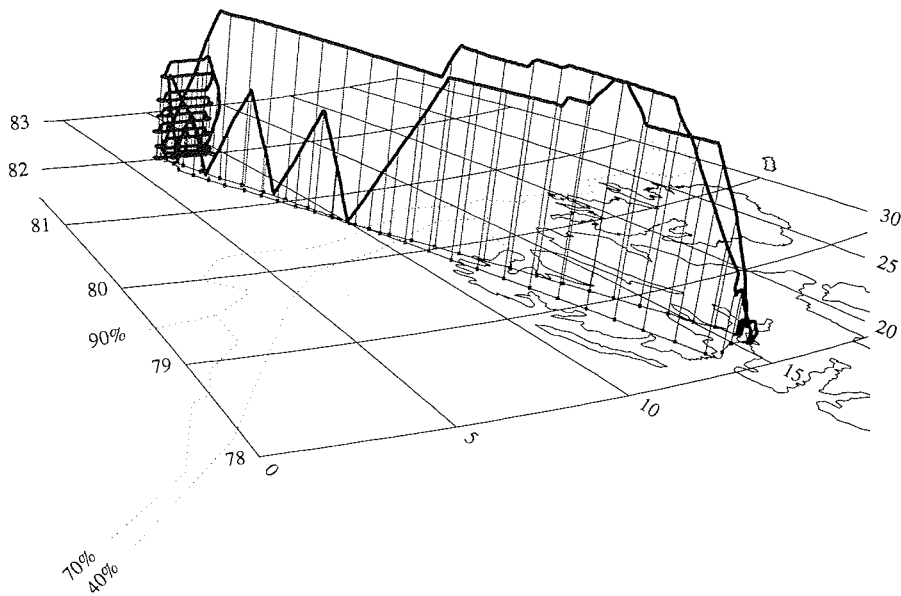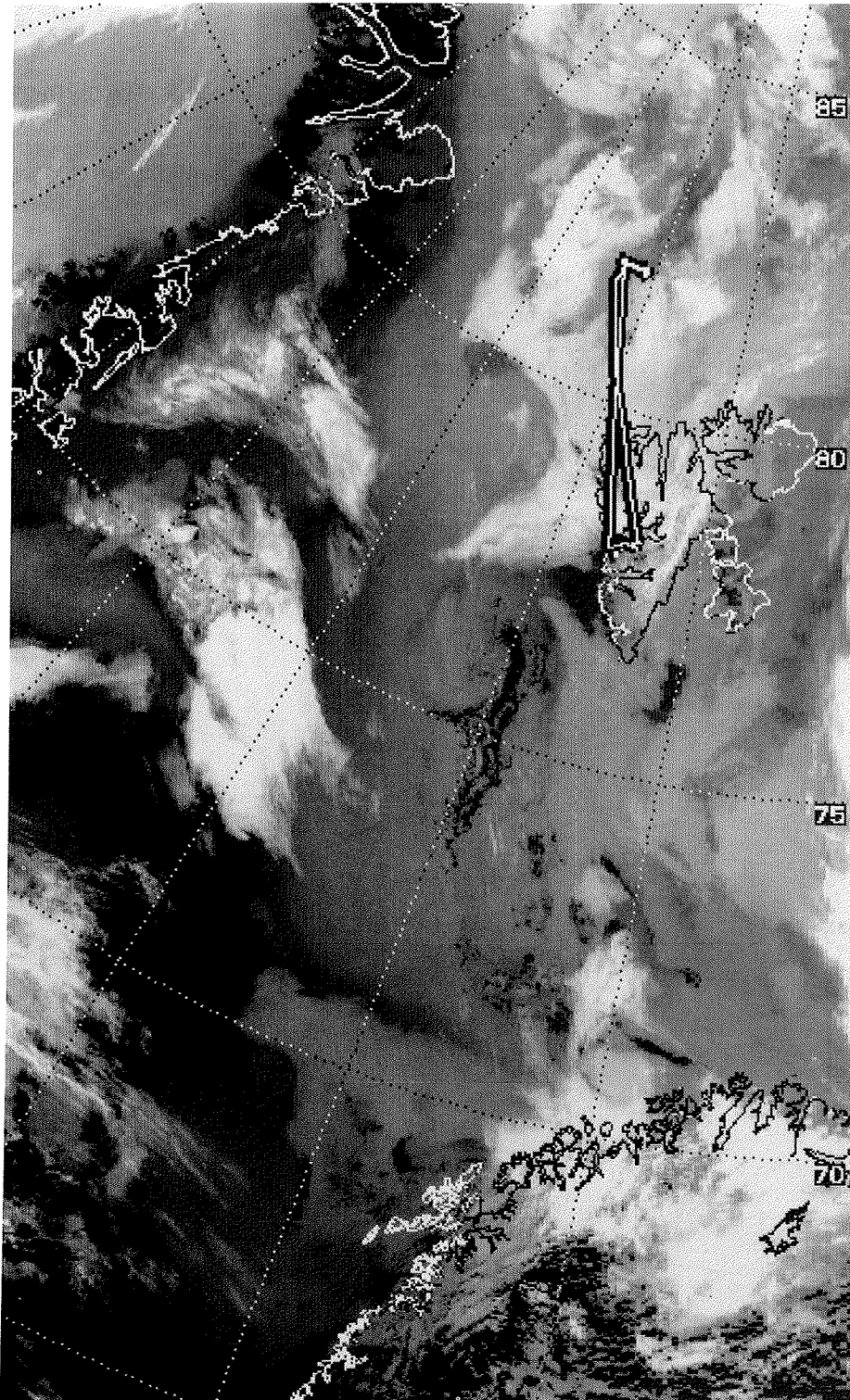
12 July 1995

A low pressure over Novaja Semlja leads to easterly winds over the ice north of
Svalbard. A warm front approaches Spitsbergen from the east.

An extended and inhomogeneous (varying optical thickness) stratus field is
present over the ice. Cloud tops range from 460 m to 900 m and cloud bases
from 150 m to 430 m. Fog patches are observed. Cirrus clouds prevent photome-
ter measurements.

The number of melt-puddles is significantly increased.

Along an L-pattern horizontal legs above and below the stratus and mainly saw-
tooth pattern are flown.

cloud tops	420 – 850 m
cloud bottom	180 – 440 m
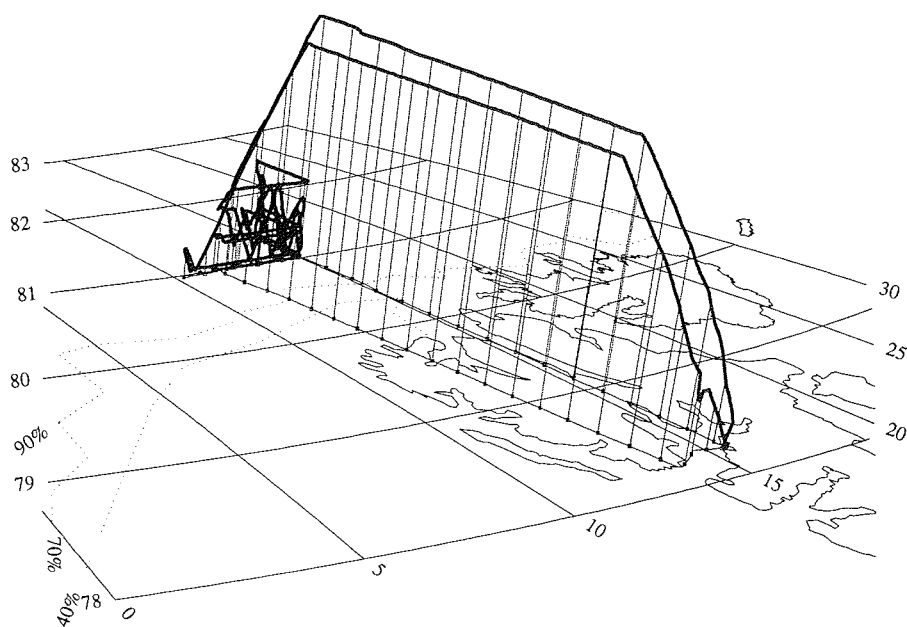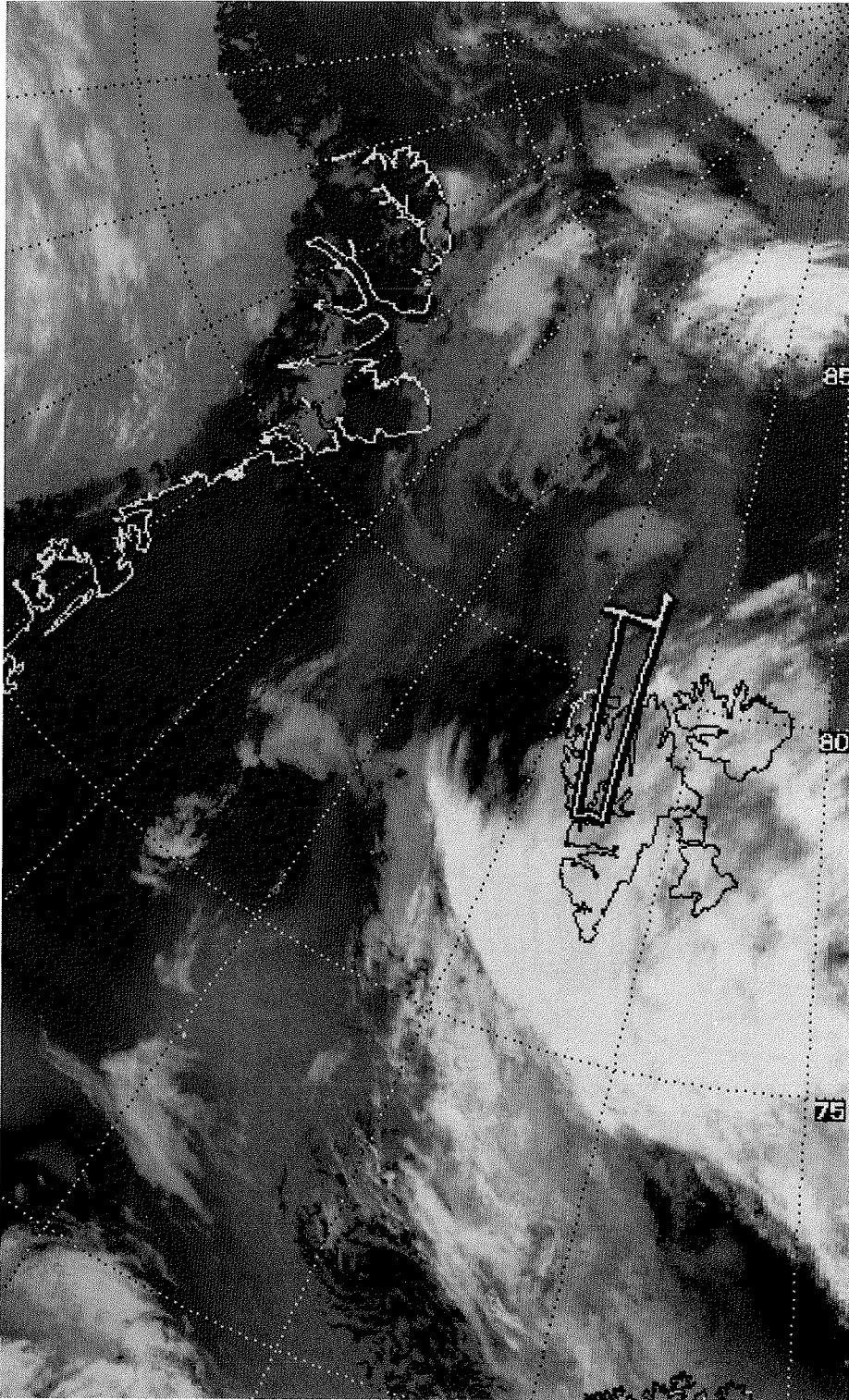
15 July 1995

A high pressure system over northern Greenland lead to northerly winds in the aerea. South of 80° N cirrus coulds moved eastward. Complex strato-cumulus and alto-cumulus were encountered over the ice. Tops were around 2000 m, cloud bases between 1000 m and 1600 m.

The flight pattern included two level flights for line scan recordings over the ice, some saw-tooth pattern through the cloud tops and photometer measurements between 60 m and 4000 m.

cloud tops	1700 – 1800 m
cloud bottom	1650 m
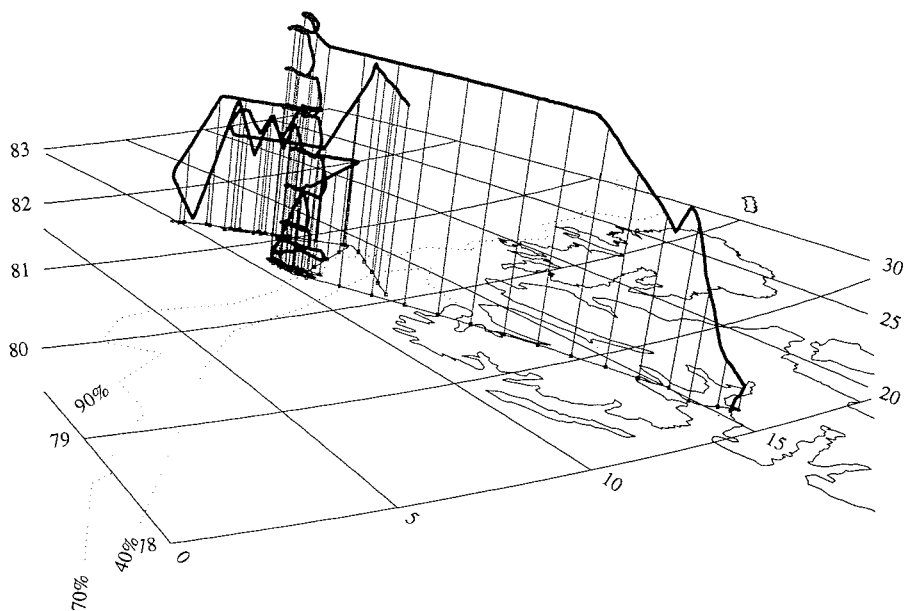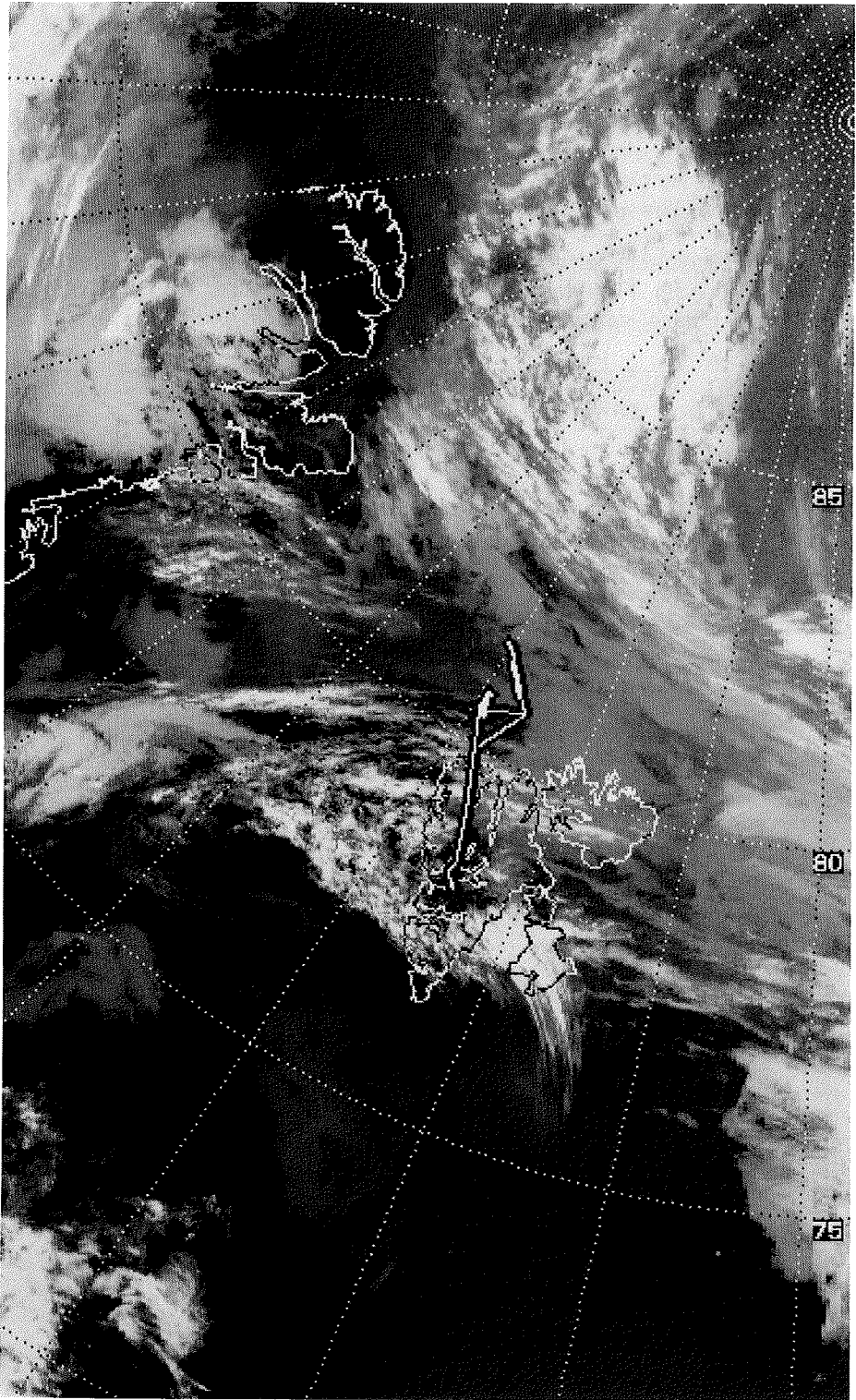
18 July 1995

The warm front of a low over Franz-Josefs-Land slowly passed from the north-
east over the region. This brought deep stratus with occasional precipitation,
weak north-easterly winds, mild temperatures and stable stratification in the mea-
surement area. No clear cloud tops were discernible, but above of 2000 m very
low particle densities were encountered.

This was the first mission of both aircraft with synchronised flights around a square
box of 15 km length. Flight levels were for Polar 2: 60 m, 30 m, 200 m, 91 m and
30 m, and for Polar 4: sawtooth, 60 m, 300 m, 450 m, 600 m and 760 m.

cloud tops	> 3200 m
cloud bottom	< 60 m
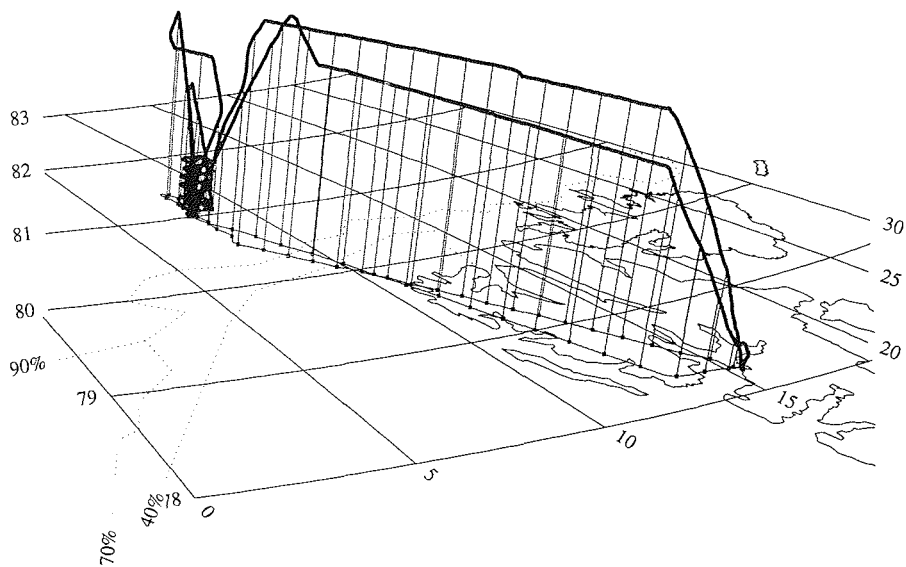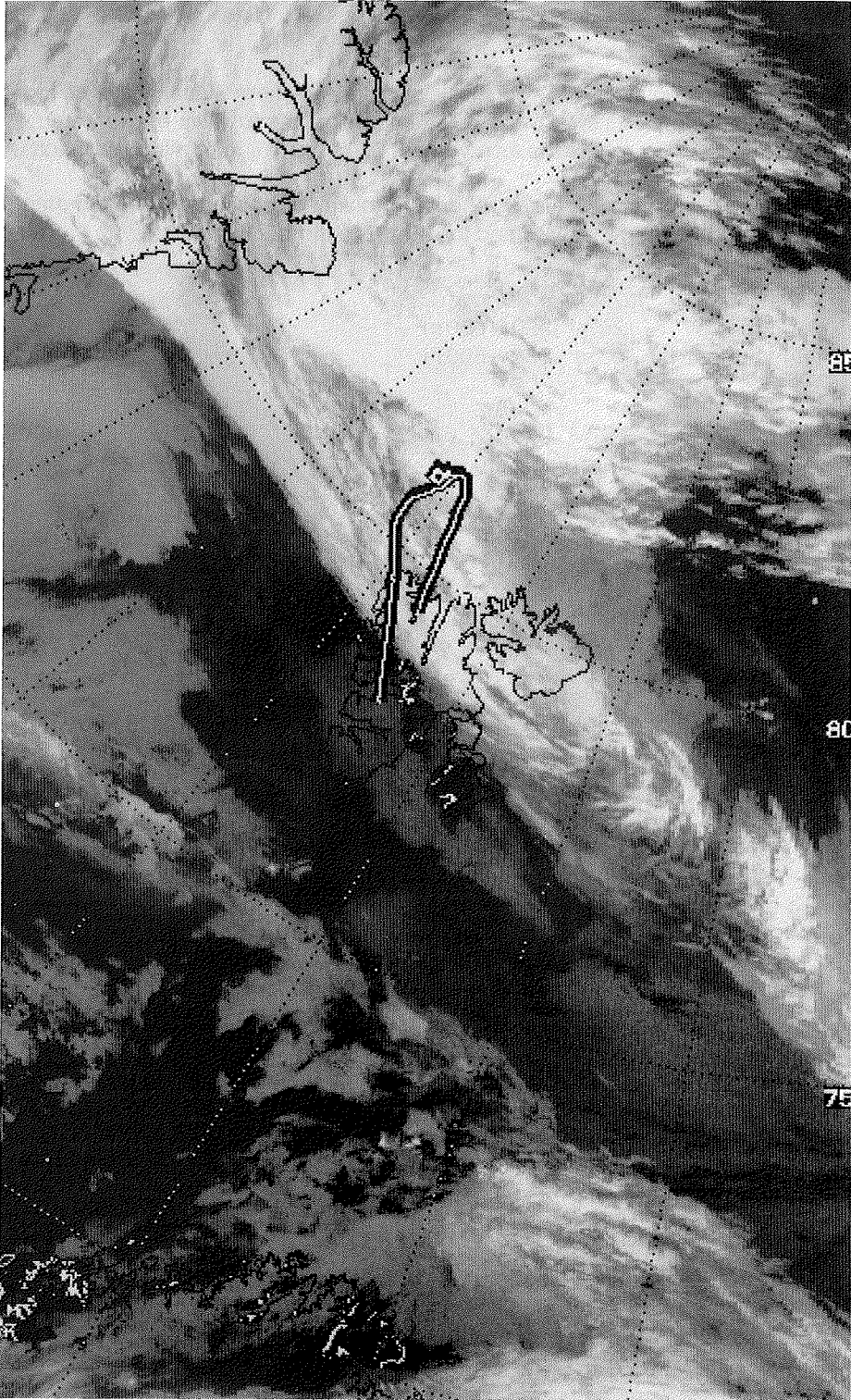
20 July 1995

After the passage of a weak front that is now over northern Svalbard the ice region was under an off-ice flow. An irregular, but typical stratus was encountered, the base touched the ground, the tops were at 600 m. No high or mid-level clouds.

A square of 15 km size was sychroneously encircled. Photometer measurements were made between Svalbard and the stratus pattern.

	layer 1	layer 2
cloud tops	120 m	420 – 650 m
cloud bottom	< 60 m	360 – 500 m
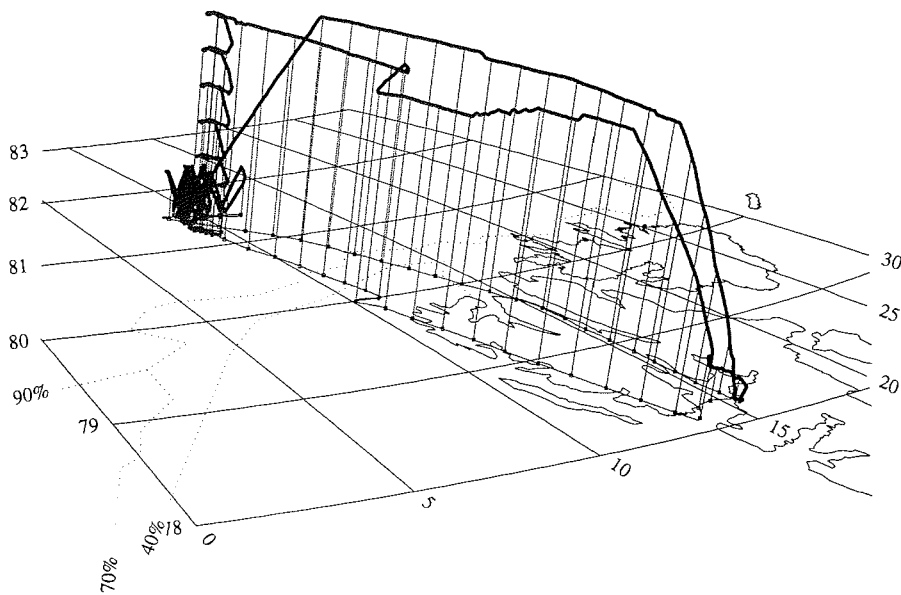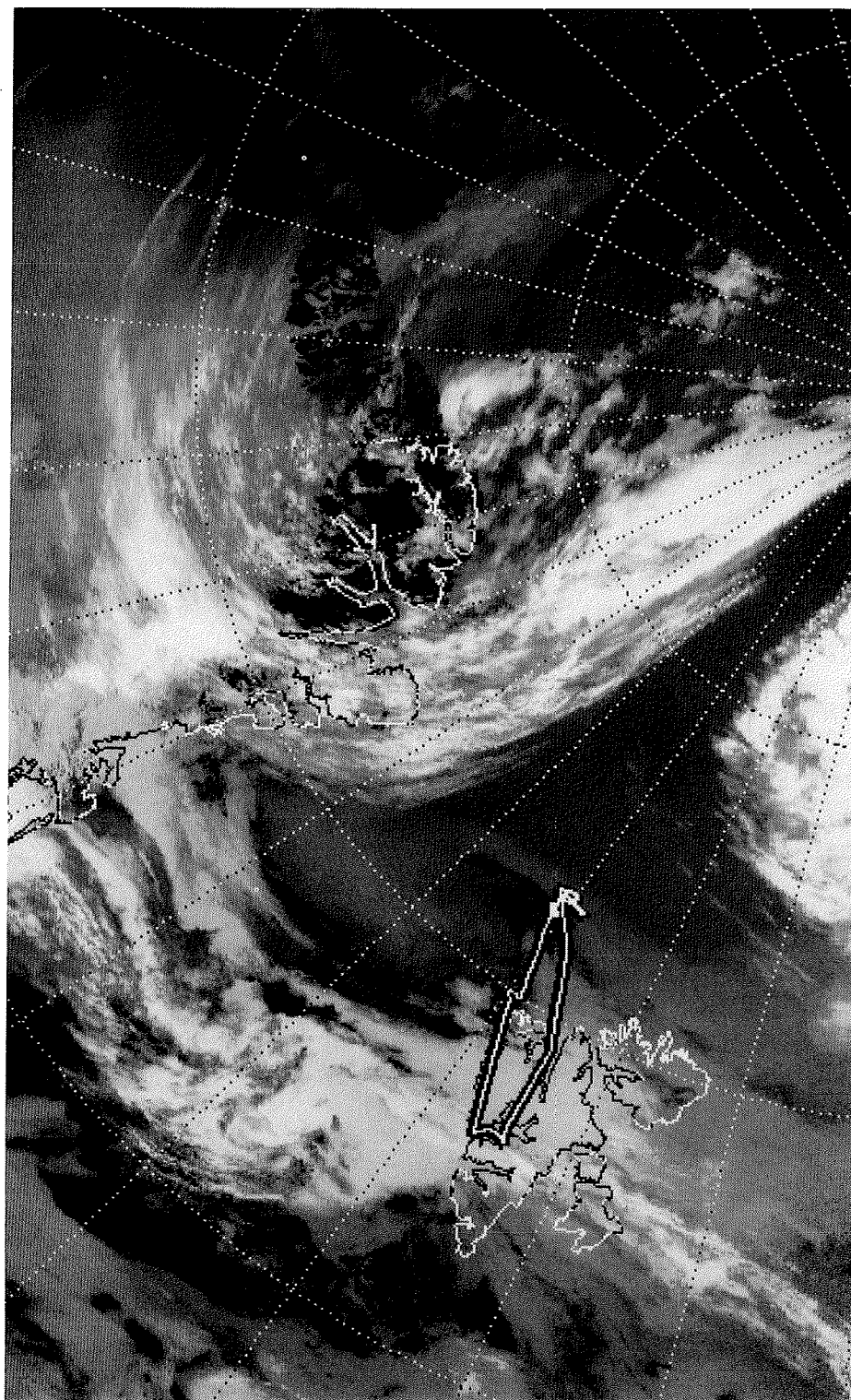
23 July 1995

A low north of Norway and a further low over the East Greenland Current lead to a south-easterly airstream in the marginal ice zone. The north-westerly part of Svalbard was cloud free, as was the ice south of 81°N. Stratus and fog was found north of 81°N.

After a synchroneous take off followed an ascent for instrument intercomparison between both aircraft. Polar2 flew a saw-tooth pattern towards the ice. Over the ice the 15km square was synchroneously circled. Additionally Polar4 flew photometer measurements and Polar2 several calibration patterns.

	layer 1	layer 2
cloud tops	150 – 180 m	1380 – 1530 m
cloud bottom	60 m	1250 – 1400 m
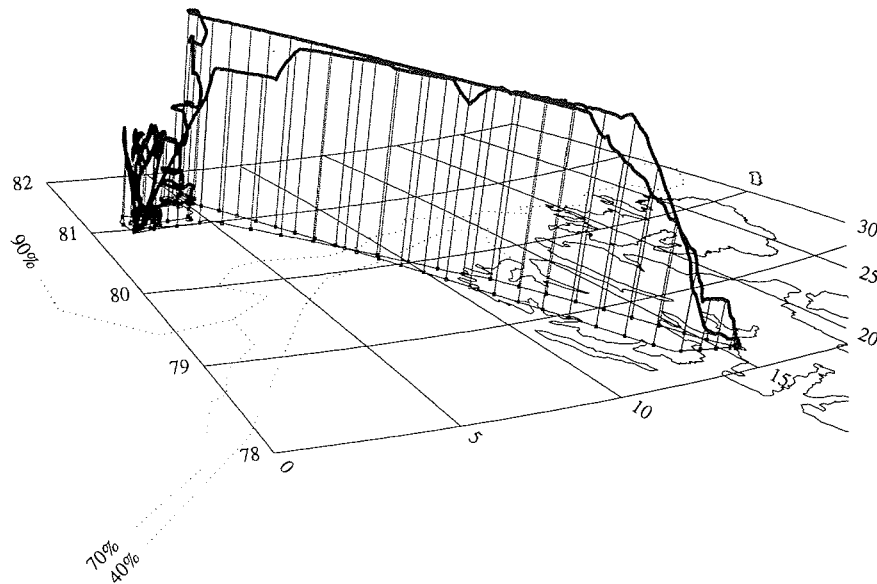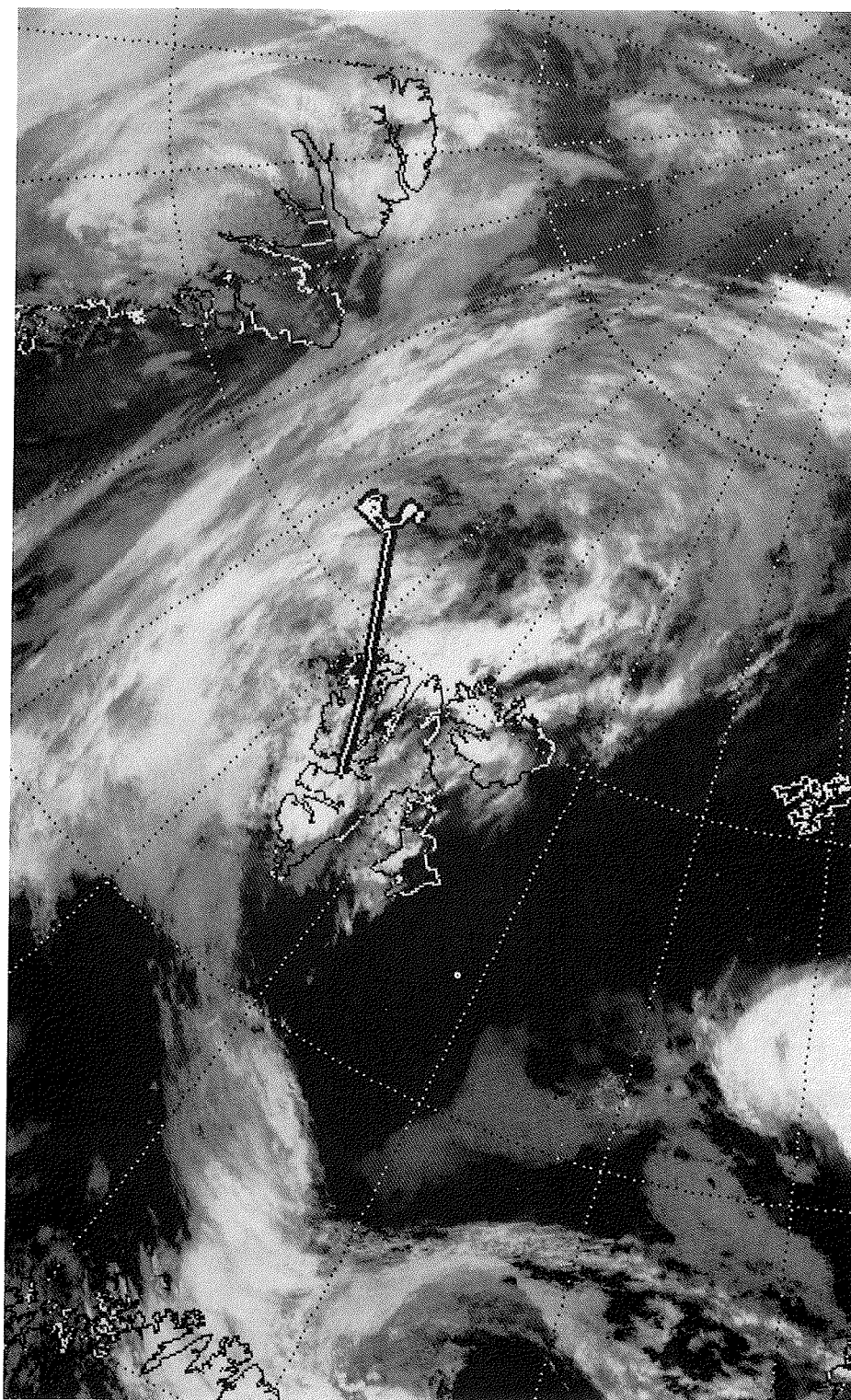
24 July 1995

A low approaching from the south-east was to bring rain in Longyear in the late
evening and led to the decision for an early start. An easterly airstream prevailed
over the ice. An extended an homogeneous stratus was found over the ice. Some
high and mid-level clouds were present.

Again, a 15 km square was encircled synchroneously. Polar 2 flew 5 circuits and
Polar 4 9 circuits.

cloud tops	270 – 330 m
cloud bottom	< 60 m
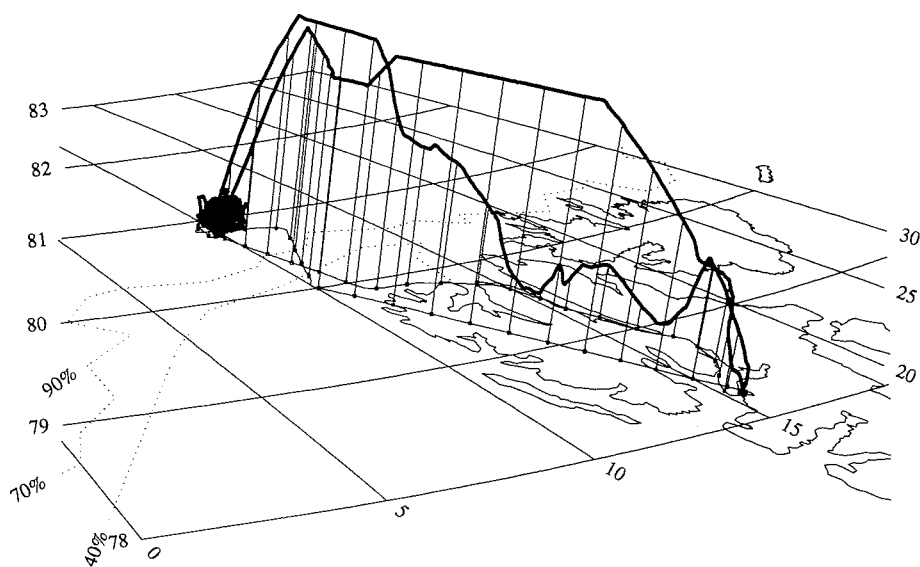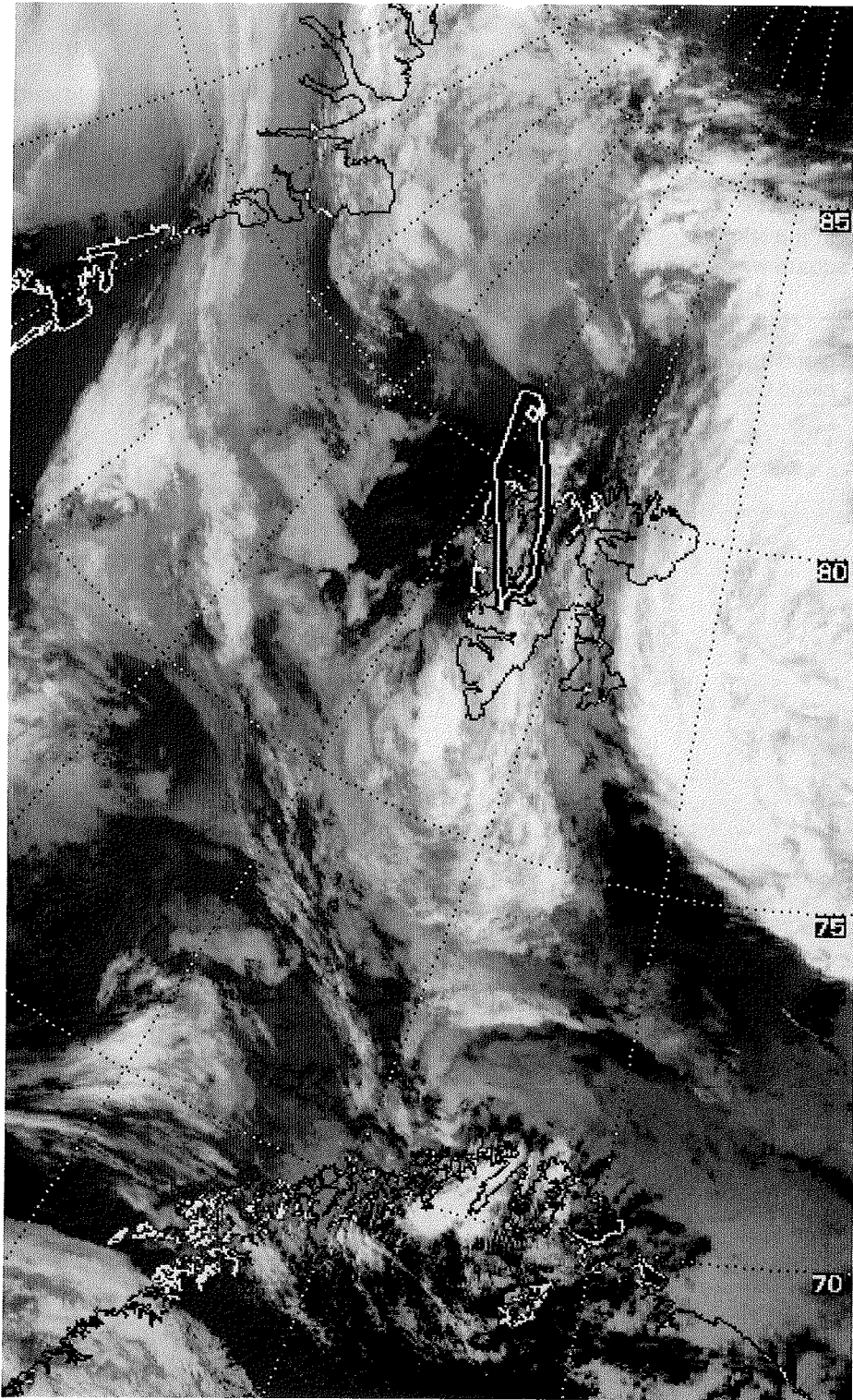
28 July 1995

A low north east of Svalbard led to westerly winds over the ice. Multilevel clouds (between 600 m and 1200 m and between 2400 m and 2700 m) were observed on the northbound track between Svalbard and the ice. There was fog over the ice and high clouds.

On the last day of REFLEX III the fifth common mission of both aircraft the 15 km square was encircled 5 times by Polar 2 and 6 times by Polar 4.

	layer 1	layer 2	layer 3
cloud tops	780 – 820 m	2230 – 2350 m	2760 – 2800 m
cloud bottom	580 – 740 m	1950 – 2150 m	2390 – 2510 m

REFLEX III
PCASP-100X
95-06-27
15:11:55 - 15:25:55
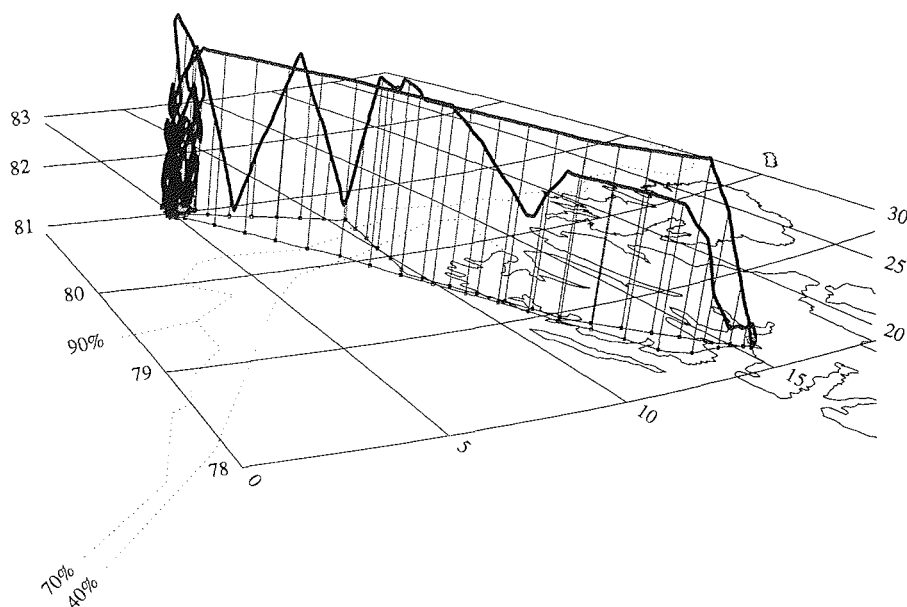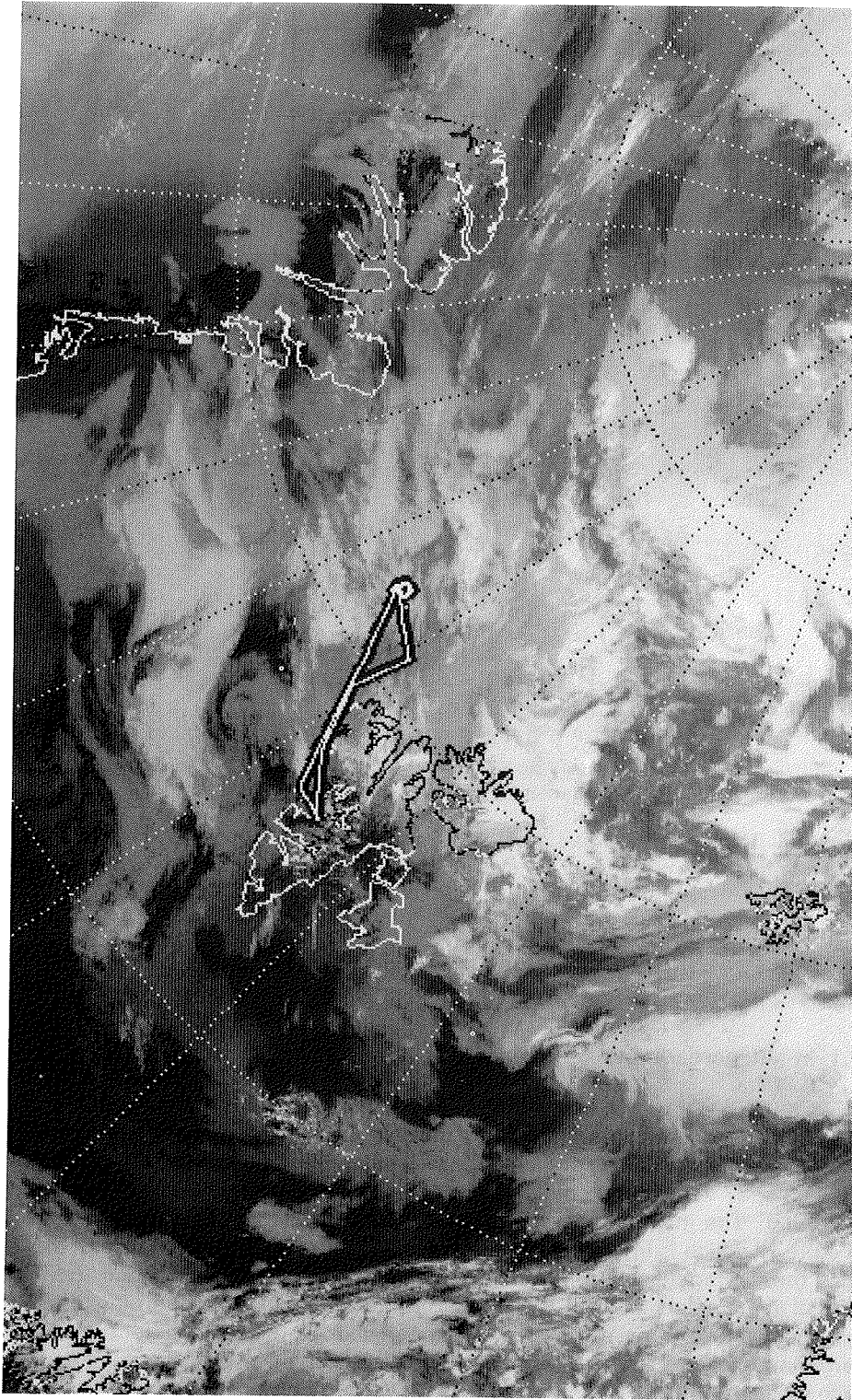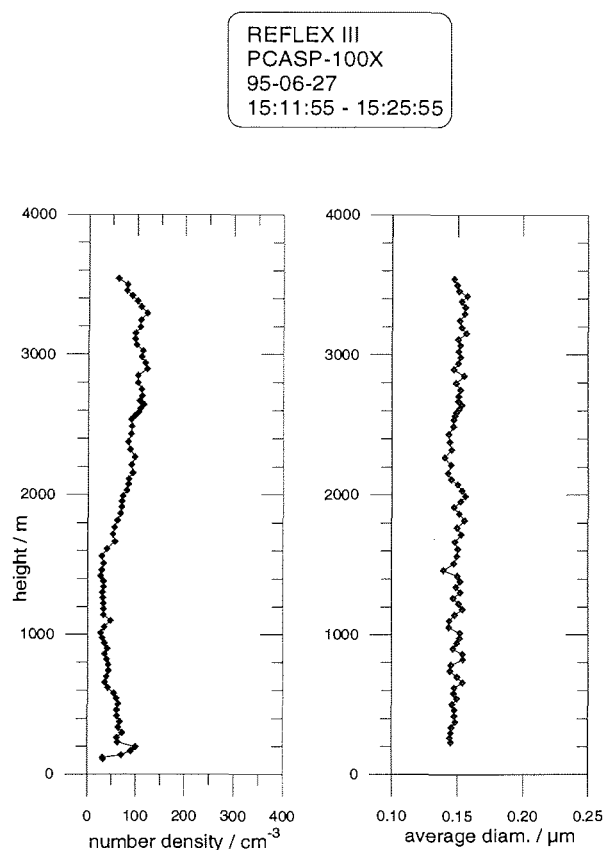
Figure 4: Number density and average diameter for a clean air case. The values are
10 s averages. The number density shows values of less than 100 cm⁻³ which is in good
agreement with literature.

6. Data Presentation

6.1. In-situ aerosol measurements

The PCASP-100X enables the determination of the number density, average dia-
meter and size distribution of aerosol particles in the range of 0.1 to 3.0 μm. During
18 flights, 37 vertical profiles of aerosol properties north of Svalbard have been
recorded. The majority of cases show number densities of less than 100 cm⁻³
(Figure 4), which is in good agreement with literature for the relative clean arctic
air. The average diameter is close to 0.15 μm. Size distribution vs. altitude for
one of these cases is given in Figure 5. The size distribution is very uniform for
altitudes up to 3600 m with the typical exponential decrease in number density for
larger aerosol sizes. The maximum of the size distribution cannot be measured
with the PCASP-100X, it is considered to be located between 0.01 and 0.1 μm.

REFLEX III
PCASP-100
95-06-17
16:19:20 - 16:39:10
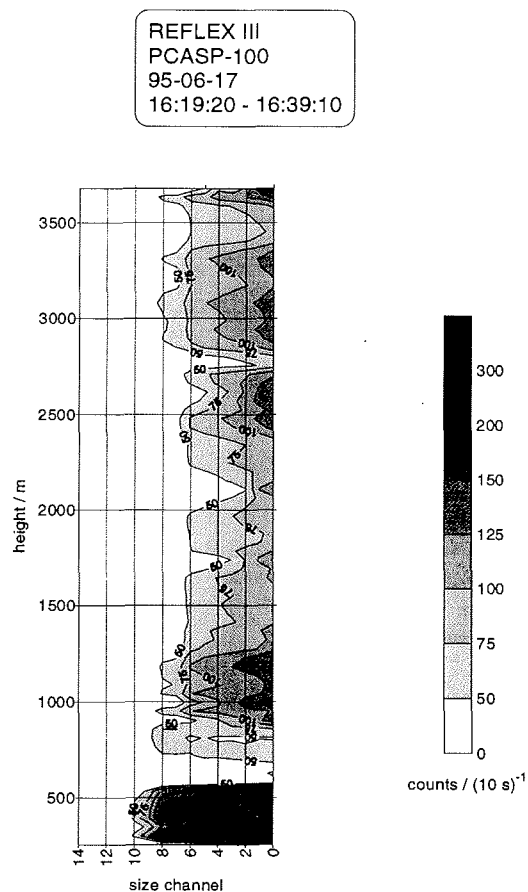
Figure 5: Aerosol size distribution vs. altitude for a clean air case. The number density is almost independent of altitude. Below 600 m there is a stratus cloud, leading to a different shape of the size distribution which is not discussed in this context.

Beside this, some arctic haze cases have been encountered even during summertime (Figure 6). One can see a significant vertical structure with a layer of almost clean air between 2200 and 2500 m. Above 2500 m, the number density increases to 800 cm^{-3} in 3400 m with a second size mode peaking at 0.22 μm (3100 m) and 0.8 μm (above 3300 m), respectively. At these altitudes, the average diameter is about 0.23 μm. Another profile with a different pattern is given in Figure 7. The vertical structure changes again at 2500 m but with constant increase of number density with altitude. Even at 4100 m, the maximum concentration is not reached. Here, no second size mode develops but most of the counts are in the smallest size channel, leading to a decrease of the average diameter down to 0.12 μm. The maximum number density is close to 1800 cm^{-3} in 4100 m which is comparable to values for central Europe. Usually, arctic haze cases are only found in spring. Therefore, these results for arctic haze cases in July are somewhat unique.

REFLEX III
PCASP-100X
95-07-04
17:19:25 - 17:59:05
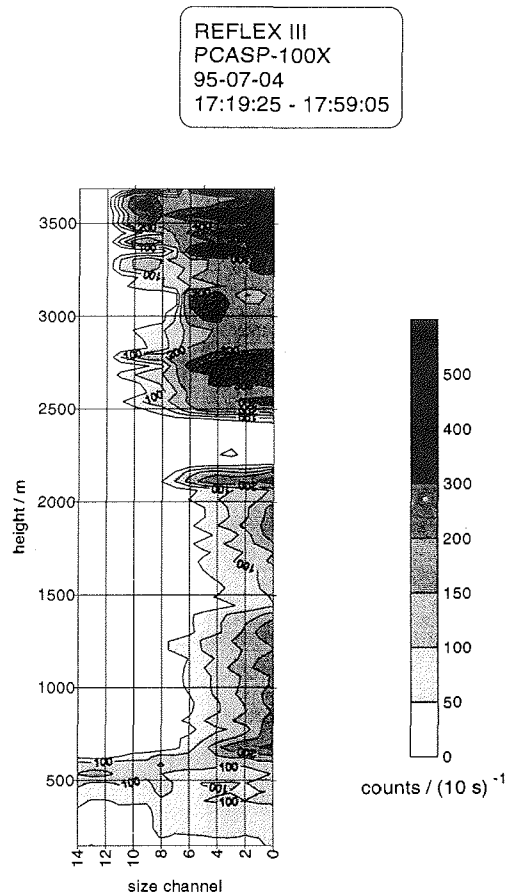
Figure 6: Aerosol size distribution vs. altitude for an arctic haze case. Above 2500 m a second size mode develops which peaks at $0.8\,\mu$m (channel 9). Below 700 m there is a stratus cloud, leading to a different shape of the size distribution which is not discussed in this context.

6.2. In-situ cloud measurements

During the arctic summer, one has to expect multilayer cloud systems in the planetary boundary layer (Figure 8). This was very frequently the case during REFLEX III. One of the striking features for many of these cloud decks was the presence of even large ice crystals up to 1.5 mm in the upper decks at temperatures between 0 and -5 C° (Figure 9). Compared to former experiments in the polar regions, the occurrence of these large crystals at relative warm environmental temperatures is unusual (J. Curry, private communication). The investigation of seeding processes of ice crystals, settling from the upper decks into the lower, pure water decks is an important task for further data analysis.

The single layered stratus which was explored during REFLEX III was very often

REFLEX III
PCASP-100X
95-07-15
15:31:30 - 16:53:40
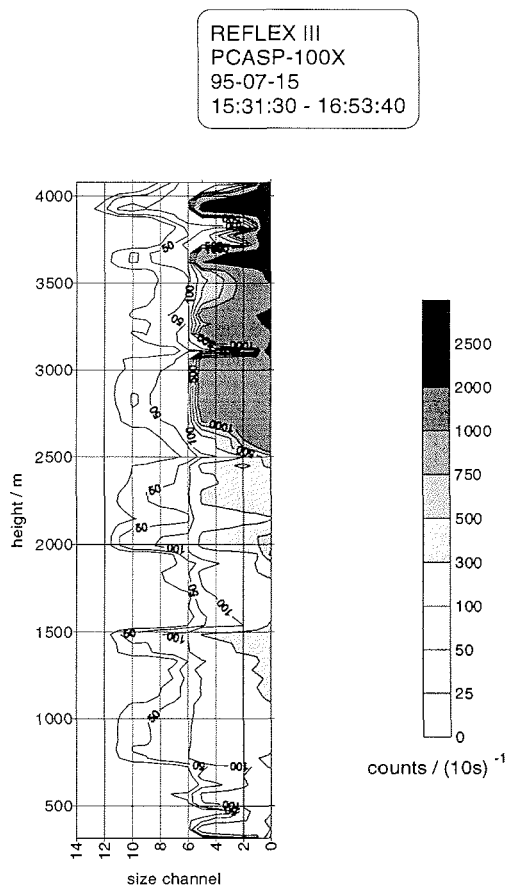
Figure 7: Aerosol size distribution vs. altitude for an arctic haze case. The number density increases up to 1800 cm^{-3} at 4100 m which is comparable with values for central Europe.

rather inhomogenous. Average values for number density, average diameter and liquid water content agree well with literature (Figure 10). The usual linear increase of diameter and liquid water content with height could be proved. Near cloud top, the variation along the horizontal flight leg shows very large variations, indicating inhomogenous structures. Individual vertical profiles taken along a distance of 15 km (Figure 11) yet differ significantly and show remarkable deviations from the horizontally averaged values. The maximum liquid water content of the profiles differs by a factor of about 2 and the height of the zone containing the maximum LWC differs from the lower third of the stratus (at 9920 m distance from point D) to the upper third of the cloud (at 1260 m distance from D). For the future, it will be analyzed whether these phenomena are related to up- and downdraft zones within the stratus or not.

The effect of inhomogeneity was further investigated by creating a cross section
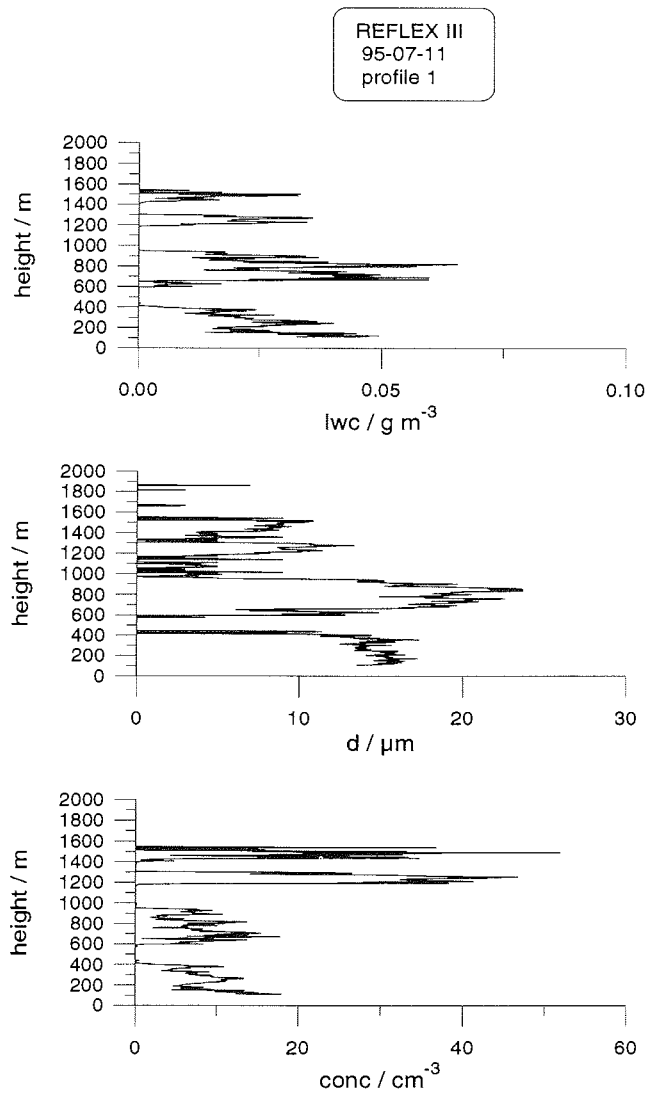
Figure 8: Example of a multilayer cloud system in the arctic during summertime. Systems like this one were very frequently encountered during REFLEX III. The upper decks often consist of ice crystals while the lower decks contain only pure liquid water droplets. From the bottom to the top, the number density, average diameter and liquid water content vs. height are shown.
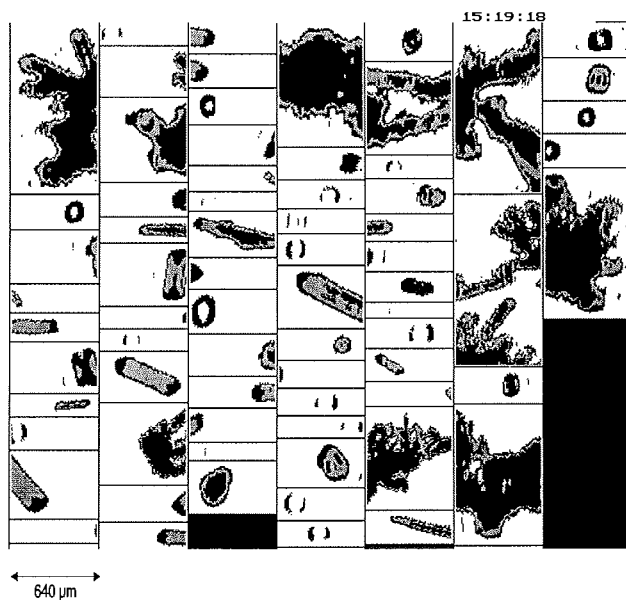
Figure 9: Example of large ice crystals, found in the upper deck of a multilayer system on July, 28th 1995 at 15:19:18 UTC.

of the stratus along the flight leg (Figure 12). It shows that the maximum liquid water content is not distributed well-balanced at a certain altitude but generates cells in the upper half of the cloud. This corresponds to the presence of cloud droplets with the maximum diameter. The number density very often shows a regular pattern of alternating zones of large and small droplet concentrations. These zones stretch from cloud base up to cloud top.

Future work strongly aims at the relation of microphysical data with radiation and turbulence data to investigate the interactions between microphysics and turbulence on the one hand and between microphysics and radiation on the other hand.
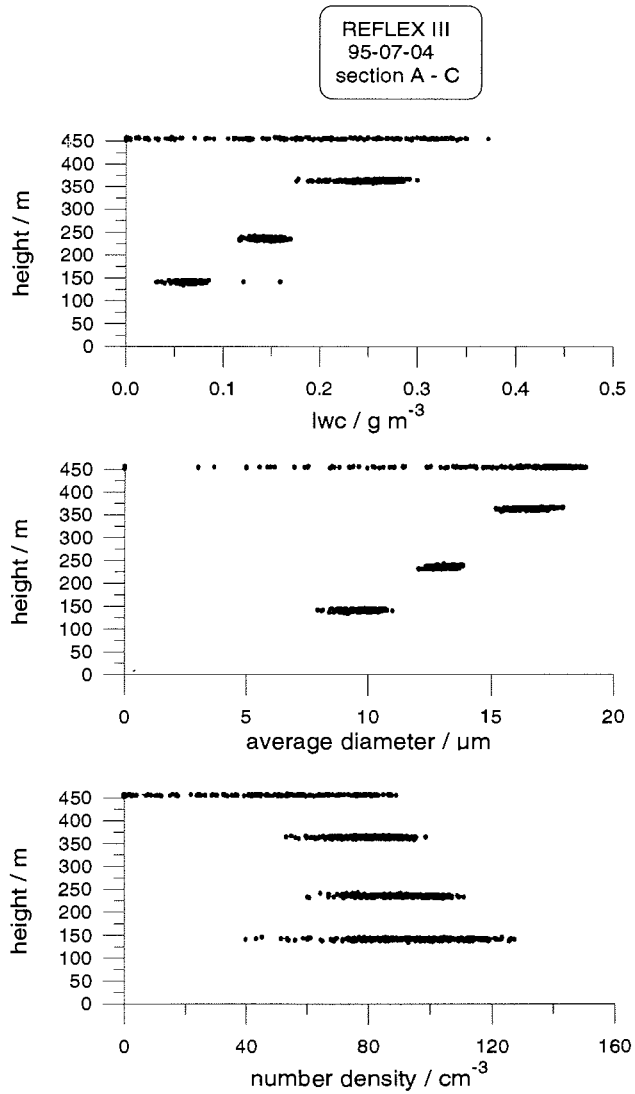
Figure 10: Number density, average diameter and liquid water content vs. height for a single layered stratus. The values agree well with literature. The linear increase of the average diameter and liquid water content with height is typical for pure water stratus clouds.
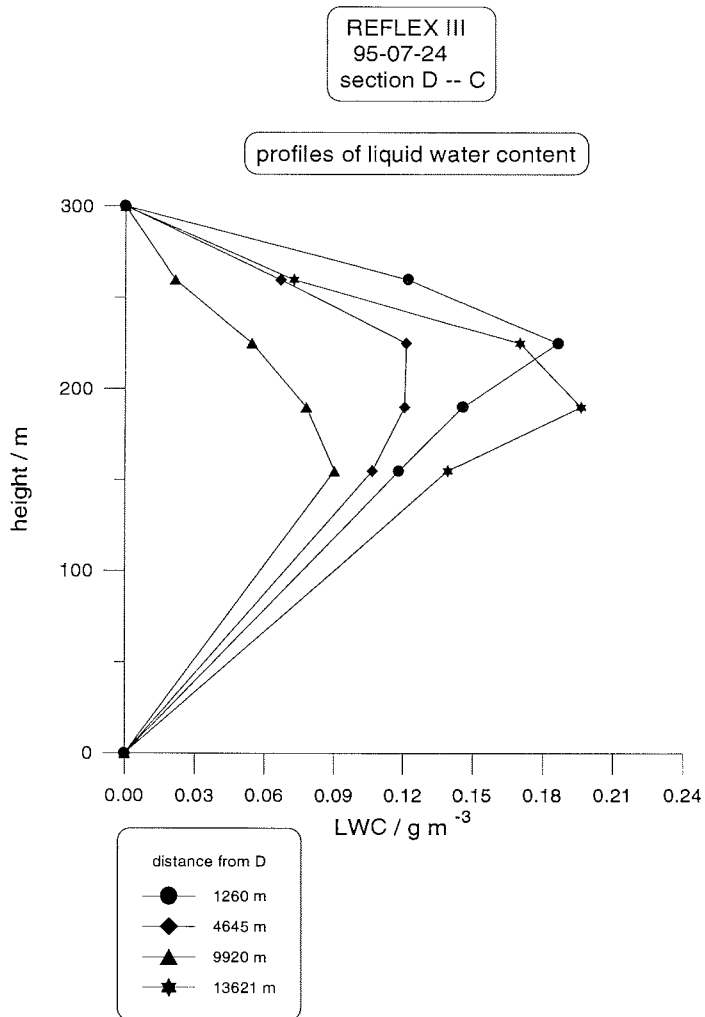
Figure 11: Individual profiles of the liquid water content along a horizontal distance of 15 km at different distances from point D (80°50'N, 10°52'E). The maximum liquid water content of the profiles differs by a factor of about 2.
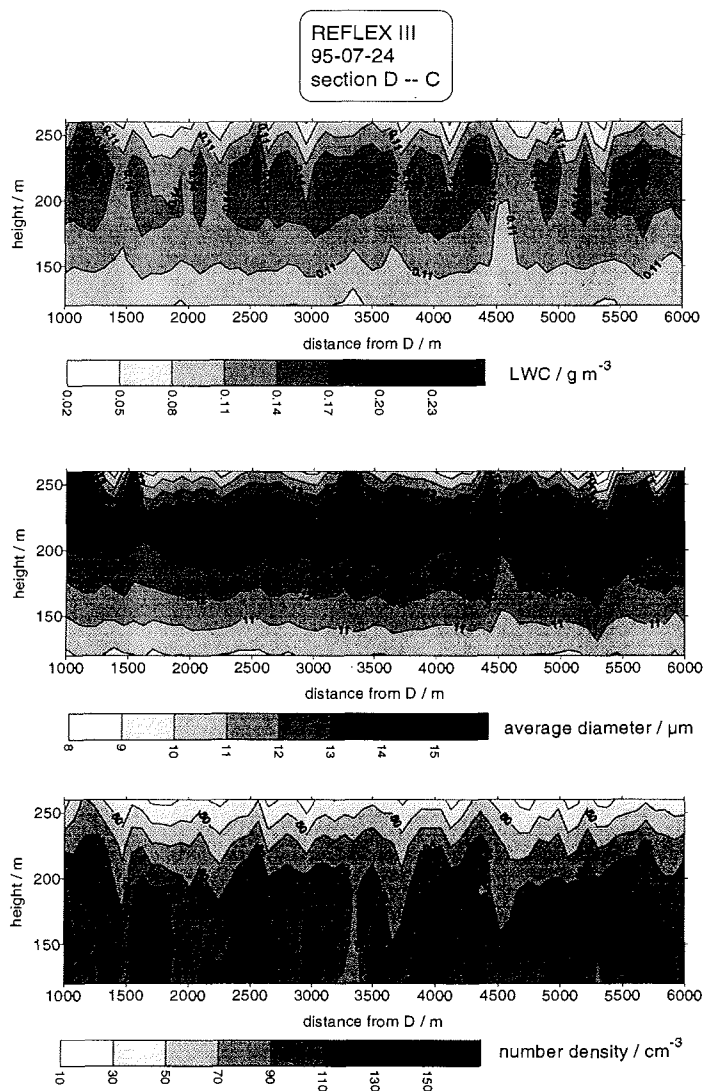
Figure 12: Cross section of a single layered stratus cloud along the flighttrack between points D (80°50'N, 10°52'E) and C (80°58'N, 10°52'E). The horizontal axis gives the distance from point D. From bottom to the top, contour plots of the number density, average diameter and liquid water content are shown for a 5 km long section of the stratus. All values are 1 s averages.

6.3. Photometer measurements

Measurements of the spectral optical thickness of aerosol were made in several flight levels in a limited geographical area. The Bouguer-Lambert' law is the basis for all calculations of the spectral optical thickness for each wavelength λ.

$$U(\lambda) = U_o(\lambda)\, e^{-\delta_T(\lambda)m} \tag{1}$$

where:

$U(\lambda)$ spectrometer signal
$U_o(\lambda)$ extraterrestrial signal
$\delta_T(\lambda)$ total optical thickness of atmosphere
m relative airmass, obtained from the actual sun elevation data

The optical thickness δ of aerosol is calculated as follows:

$$\delta_{Ae}(\lambda) = \delta_T(\lambda) - \delta_{Ray}(\lambda) - \delta_{O_2}(\lambda) - \delta_{O_3}(\lambda) - \delta_{NO_2}(\lambda) - \delta_{H_2O}(\lambda) \tag{2}$$

where the subscipts denote:

Ae = aerosol
Ray = atmosphere due to Rayleigh scattering
O_2 = oxygen
O_3 = ozone
NO_2 = nitrogen dioxid
H_2O = water vapour

From this data a calculation of the spectral extinction coefficient in every layer was possible to get finally a vertical distribution of the aerosol.

Examples

The first example from 25 June 1995 shows a typical aerosol profile in summer time (Figure 13), as we measured it for the most part. Aerosol optical thickness does not exceed 0.055 and the extinction coefficient is less than 0.04 km^{-1}. The aerosol is concentrated in the boundary layer. At a height of about 2.5 km it is more or less zero. The small layers of larger aerosol particles, represented by the wavelength of 1057 nm, correspond to the high amount of relative humidity. They indicate the presence of natural aerosols, for instance sea salt.

The second example in Figure 14 shows an untypical haze event on 4 July 1995. Measurements started in a height of about 700 m above cloud tops (compare relative humidity of 100%). In the thin layers, which were also visible as dark brown

(78,8° - 79°) N ; (6° - 6,8°) E
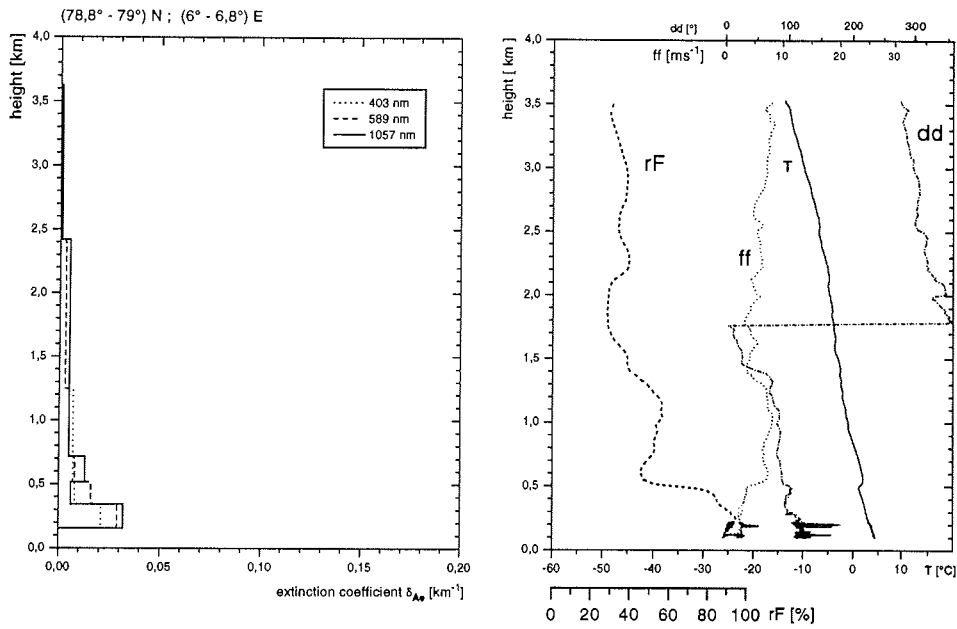
Figure 13: Vertical aerosol profile and meteorological parameters on 25 July 1995. T is temperature, dd wind direction, ff wind speed and rF relative humidity.

(79,4° - 81°) N ; (2° - 4,1°) E
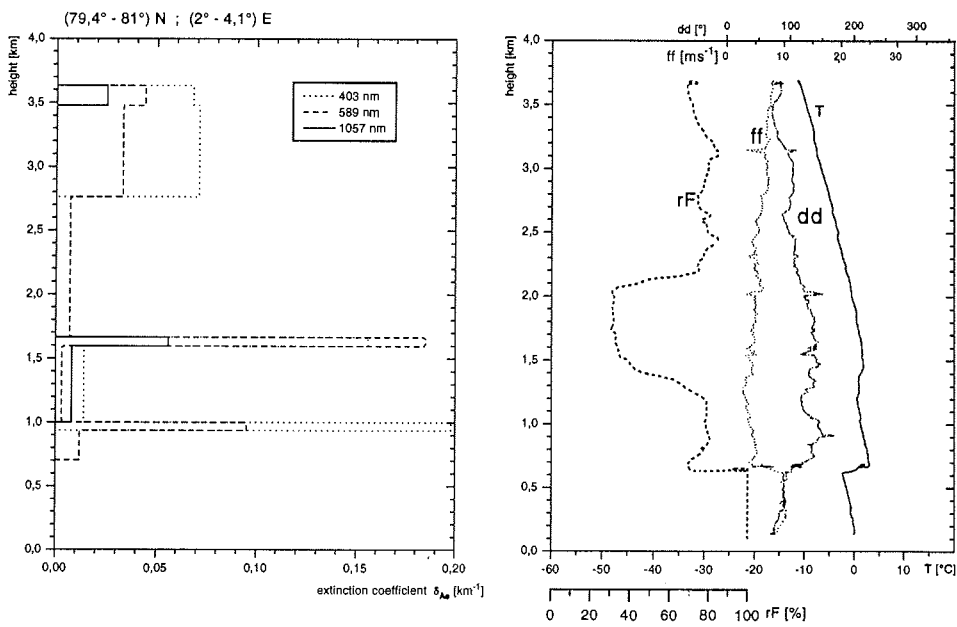
Figure 14: Vertical aerosol profile and meteorological parameters on 4 July 1995. T is temperature, dd wind direction, ff wind speed and rF relative humidity.

layers, small aerosols, represented by the wavelength of 403 nm, dominate. This high extinction coefficients of about 0.2 km^{-1} do not corresponde to the relative humidity. The maximum optical thickness was 0.3 at a wavelength of 403 nm, a value normally found in Central Europe. The higher aerosol concentration (extinction coefficient $> 0.05 km^{-1}$) was measureable up to the top flight level. There are grounds for the supposition that this aerosols represent an anthropogenic pollution.
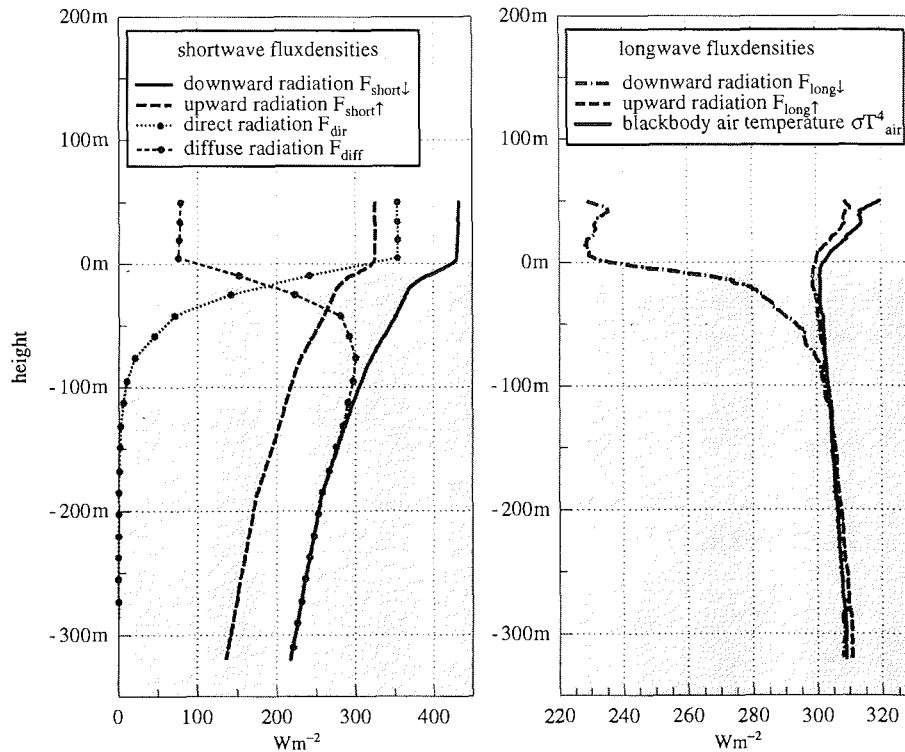
Figure 15: Left: the diffuse and direct part of the global radiation and the reflex radiation in a stratus cloud over polar surface. Right: the longwave up- and downward radiation and the blackbody air temperature inside a stratus cloud. The ordinate represent the distance to the cloud top.

6.4. Radiation Measurement

The instrumental equipment comprised Eppley pyranometers and pyrgeometers to measure the solar and terrestrial up- and downward hemispheric radiation flux densities. With this information we are able to determine the radiative energy exchange between the sea ice covered ocean and the arctic atmosphere.

Two examples of these measurements show the influence of radiation on the atmospheric longwave cooling and shortwave heating rates.

Radiation profiles in a stratus cloud over sea-ice

On July 4, 1995 a stationary flow from the ocean to the ice transported moist air to the measurement area. We found a low stratus cloud with cloud tops from 425 to 525 m. Profiles of the short and long wave flux densities are schown in
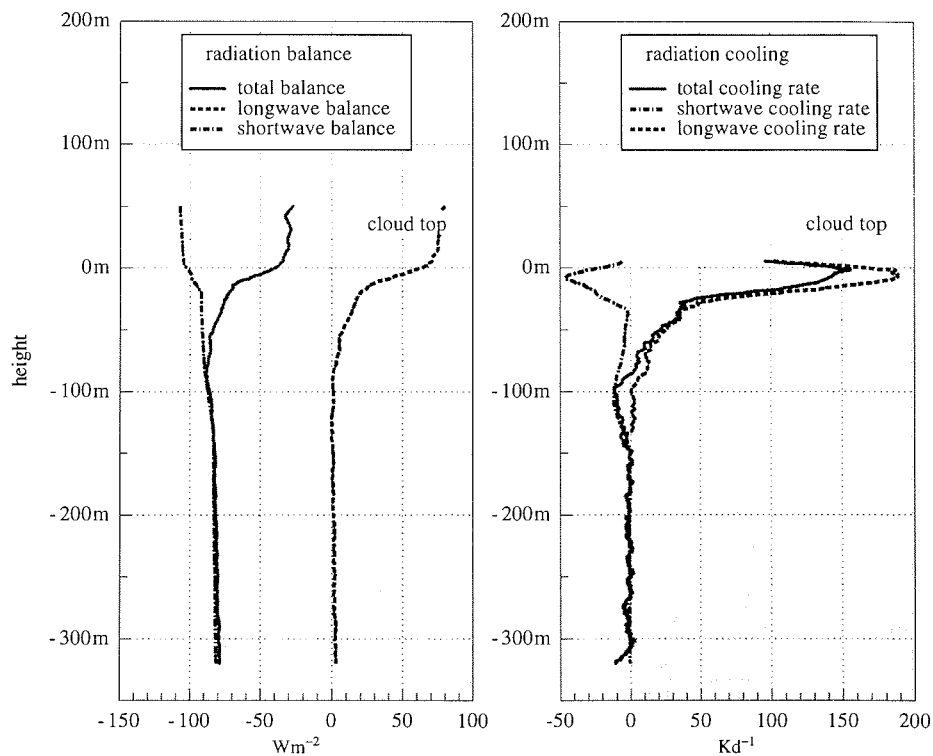
Figure 16: Left: profiles of the radiation balances for the status case. Right: the shortwave, longwave and total cooling rates inside the cloud. The ordinate represent the distance to the cloud top.

Figure 15. The radiation measurements are corrected for the aircraft movement. Furthermore, the perpetual small variation of the aircraft attitude allows to split the global radiation into its diffuse and direct part. For comparison the longwave radiation emmitted by the atmosphere, σT^4_{air}, is also plotted. Inside the cloud the, downward and upward longwave radiation are equal, we have $F_{long,\uparrow} = F_{long,\downarrow} = \sigma T^4_{air}$.

Figure 16 shows the profiles of the radiation balance and the resulting heating and cooling rates.

The short wave heating rate reaches its maximum at the cloud top due to the maximum liquid water content and the low sun elevation. The high emissivity of the stratus cloud causes a large longwave cooling rate that dominates the total radiation balance.

At the cloud bottom the liquid water content is small and the surface temperature is higher than the near surface air temperature. Thus the upward longwave radiation is slightly higher then the blackbody temperature just above cloud bottom. This effect is connected with a small amount for the longwave heating rate. The atmo-
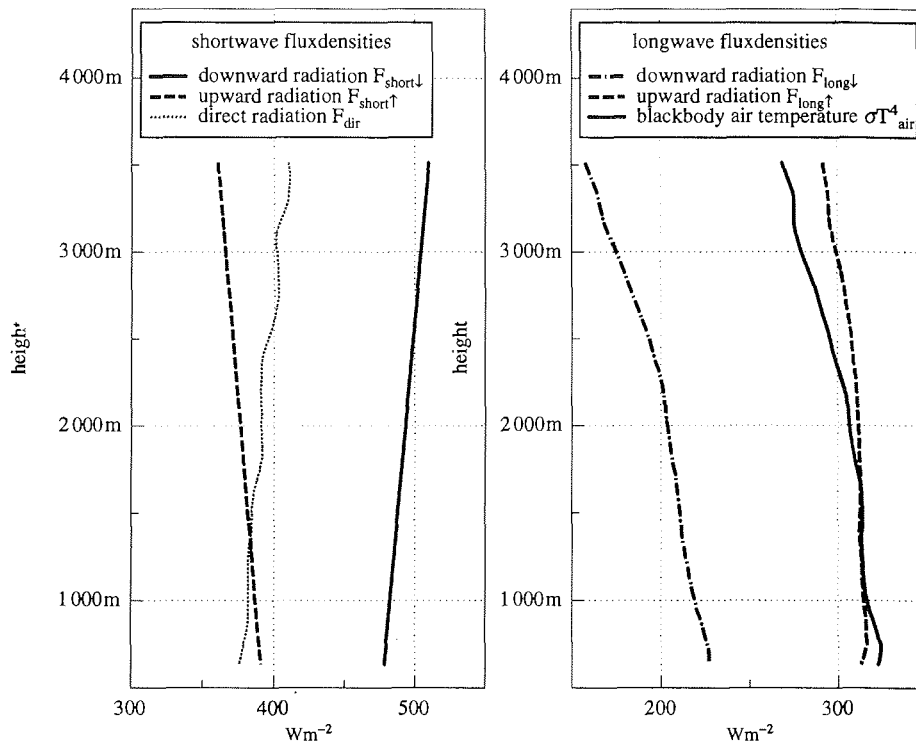
Figure 17: Left: profiles of the global, direct and the reflex radiation in an arctic air mass with an aerosol content. Right: the longwave up- and downward radiation and the atmospheric long wave emmision derived from the air temperature by σT^4.

spheric counter radiation reaching the surface equals the blackbody temperature at 310 m below the cloud tops.

The radiation energy balance at the surface results in a total of 80 W/m² flux to the surface. This energy is available for ice melting. The cloud loses nearly 45 W/m² due to raditive cooling. This correspond to a cooling rate of 8.6 K/d for the entire cloud layer. Because of the large cooling at the cloud top and a small heating at the cloud bottom the radiation has a destabilising effect.

Radiation aerosol profile over arctic stratus clouds

For small optical thickness τ like aerosol-layers, the derivations from the shortwave radiation flux densities are nearly constant. Thus the radiation profile is in the first order nearly linear with height.

The measured upward and downward radiation profiles (Figure 17) are typical for the arctic atmosphere with an aerosol content. Because of the small single
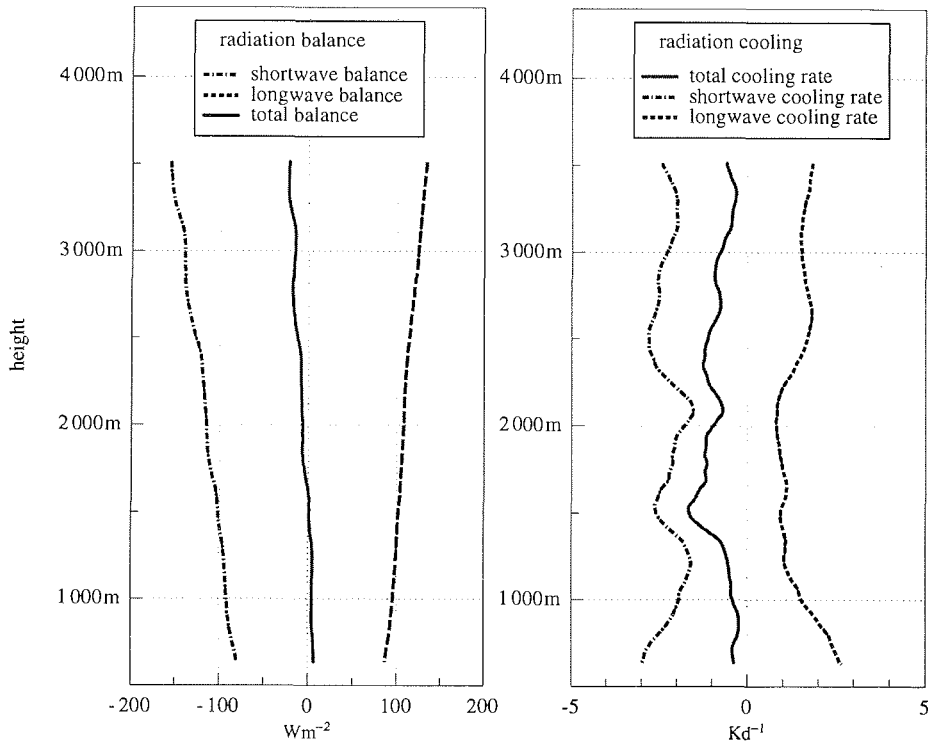
Figure 18: Left: Profiles of the short and long wave and the total radiation balance. Right: the shortwave, longwave and total cooling rate.

scattering albedo in some wavelength bands and the high stratus cloud albedo the upward shortwave radiation decreases with height. Because of isolated aerosol layers the direct radiation changes its intensity at 3300 m, 2500 m, 1600 m and 900 m. The mean shortwave heating rate amounts to 2.3 K/d for the layer from 600 m to 3500 m. In the aerosol layers the heating rate increase up to 3 K/d.

The longwave cooling profile looks more smoothly (Figure 18). Above 2500 m the longwave cooling rate has an amount of 1.8 K/d. Between 1200 and 2500 m the value drops to 1 K/d, but below 1200 m the longwave cooling rate increase up to 3 K/d.

The longwave cooling rate is of the same magnitude as the shortwave heating rate so the mean total effect is nearly zero. On that time, the shortwave heating rate is predominant so the sum has an total amount of 0.5 K/d with a maximum of 1.8 K/d at 1500 m.
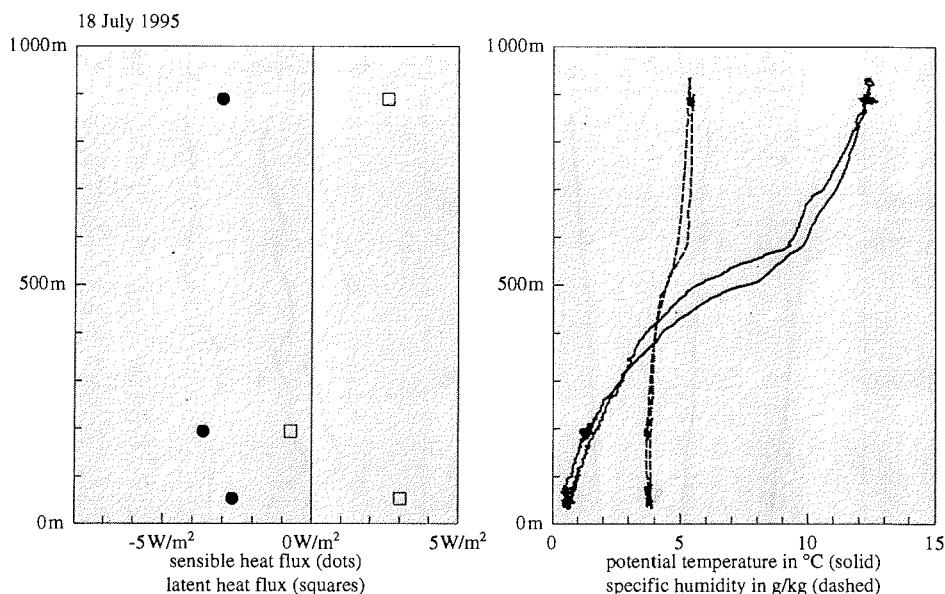
Figure 19: Left: vertical profiles of the sensible heat flux and the latent heat flux. The symbols represent averages over all legs at one flight level. Right: vertical profiles of the potential temperature and the specific humidity.

6.5. Turbulence

In the arctic summer the frequent advection of relatively warm and moist air over melting sea ice leads to stable stratification, low stratus clouds and small downward heat fluxes. During REFLEX III a good example of such a case was encountered on 18 July 1995. Both aircraft flew a square pattern over the ice, Polar 2 mainly level flights for turbulence measurements, Polar 4 mainly ascents and descents for radiation and cloud physics studies. In Figure 19 profiles of the potential temperature, the specific humidity and the sensible and latent heat flux are shown.

In the stably stratified air downward sensible heat fluxes of about 3 W/m² were measured by Polar 2. Since the air above 500 m height was significantly warmer than the surface, the downward longwave radiation exceeded the upward longwave radiation by about 5 W/m². The largest surface heating of about 50 W/m², however, resulted from the short wave radiation balance.

It is interesting to examine the scales and variability of the downward heat flux in different heights. Figure 20 shows the flight tracks of Polar 2 together with the instantaneously calculated sensible heat flux. At low altitudes a small downward heat flux occurs regularly over all four legs of the square pattern. With increasing altitude larger local fluxes occur, but the irregularity increases. As Figure 19 shows the average heat flux at 889 m height is nearly the same as that at 49 m height.
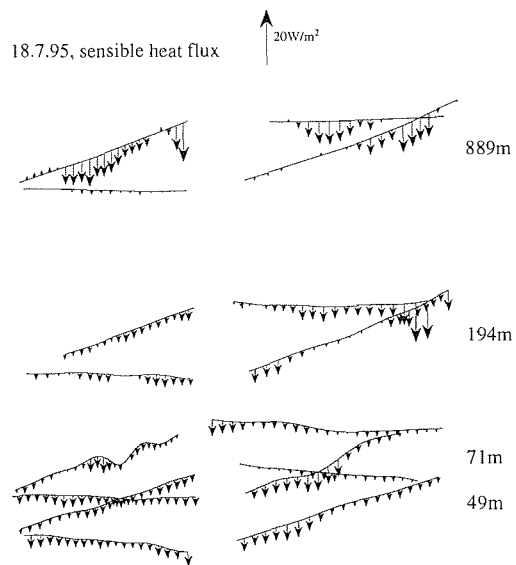
Figure 20: Flight tracks of Polar 2 and an arraw representation of the instantaneous sensible heat flux.

As a second example a heat flux profile for a case with a stratus cloud cooled by radiation at the top is shown in Figure 21. A downward sensible heat flux of 10 W/m^2 is measured at the top of the stratus cover. At this height the temperature profile shows the strongest stability. The solid lines in the right graph of Figure 21 represent three vertical transects of the could top. Note that the height of the strongest temperature gradient varies by about 50 m.

24 July 1995
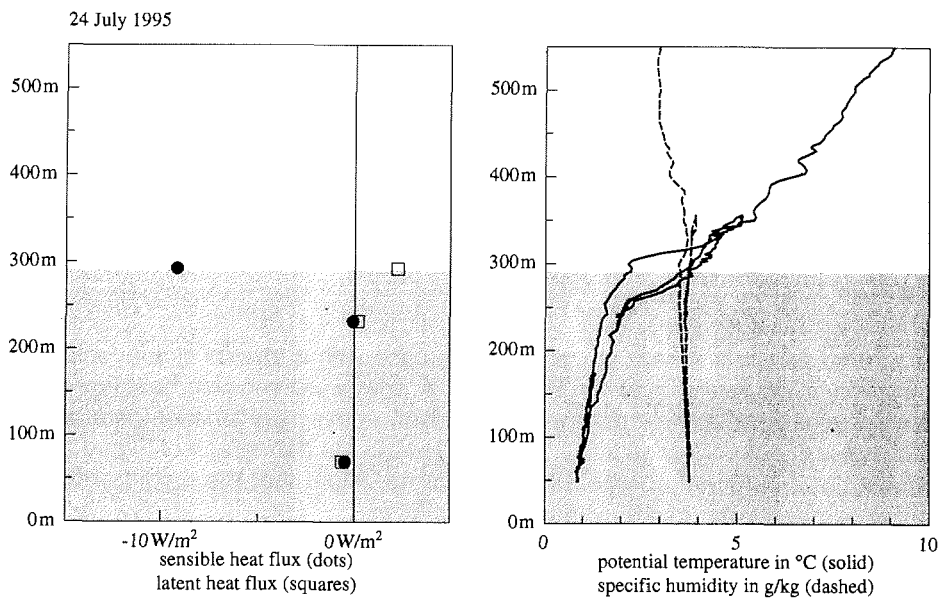
Figure 21: Left: vertical profiles of the sensible heat flux and the latent heat flux. The symbols represent averages over all legs at one flight level. Right: vertical profiles of the potential temperature and the specific humidity. The grey shading in both graphs marks the height range of the stratus cloud.

7. References

Bochert, A. and Holzschuher, R., 1995: *Einsatz des Color-Line-Scanners.* Alfred-Wegener-Institut. Bremerhaven.

Bochert, A. and Wamser, C., 1994: New Airborne Line Scanner Systems for High Resolution Sea Ice Observation. *The Global Atmosphere and Ocean System.* Vol. 2. pp. 247–251.

Gardiner, B.A. and J. Hallet, 1985: Degradation on In-Cloud Forward Scattering Spectrometer Probe Measurements in the Presence of Ice Particles, *J. Atmos. Oceanic Technol.*, **2**, 171–179

Hartmann, J., Kottmeier, C. and Wamser, C., 1992: Radiation and Eddy Flux Experiment 1991 (REFLEX I). *Berichte zur Polarforschung*, **105**.

Kottmeier, C., Hartmann, J., Wamser, C., Bochert, A., Lüpkes, C., Freese, D. and Cohrs, W., 1994: Radiation and Eddy Flux Experiment 1993 (REFLEX II). *Berichte zur Polarforschung*, **133**.

Leiterer, U. and Weller, M., 1988: Sunphotometer BAS and ABAS for atmospheric research, WMO Tech. Doc., 222, 21–26.

Leiterer, U. and Weller, M., 1993: Verfahren zur Bestrahlungsstärke- und Strahldichtekalibrierung von Spektrometern und Sonnenphotometern des Typs BAS, Meteorol. Zeitschrift, N.F.2, 108–115.

Reuter, A., 1994: *Zur Ableitung von Partikelgrößenverteilungen mit einer 2D-Greyprobe*, thesis in meteorology, Institut für Geowissenschaften der Universität Hamburg.

8. Acknowledgements